HHS Public Access

Author manuscript

FASEB J. Author manuscript; available in PMC 2022 September 01.

Published in final edited form as:

FASEB J. 2021 September ; 35(9): e21788. doi:10.1096/fj.202100397R.

Mechanisms linking hypoxia to phosphorylation of insulin-like growth factor binding protein-1 in baboon fetuses with intrauterine growth restriction and in cell culture

Jenica Kakadia[1], **Kyle Biggar**[2,$], **Bhawani Jain**[1,$], **Allan W Chen**[1], **Karen Nygard**[3], **Cun Li**[4,5], **Peter W Nathanielsz**[4,5], **Thomas Jansson**[6,#], **Madhulika B Gupta**[1,7,8,#,*]

[1]Department of Biochemistry, University of Western Ontario, London, ON, Canada;

[2]Institute of Biochemistry, Carleton University, Ottawa, ON, Canada;

[3]Biotron Integrated Microscopy Facility, University of Western Ontario, London, ON, Canada'

[4]University of Wyoming, Laramie, WY, USA;

[5]Southwest National Primate Research Center, San Antonio, TX, USA;

[6]Department of Obstetrics and Gynecology, Division of Reproductive Sciences, University of Colorado Anschutz Medical Campus, Aurora, CO, USA;

[7]Children's Health Research Institute, London, ON, Canada;

[8]Department of Pediatrics, University of Western Ontario, London, ON, Canada.

Abstract

Hypoxia increases fetal hepatic insulin-like growth-factor binding protein-1 (IGFBP-1) phosphorylation mediated by mechanistic target of rapamycin (mTOR) inhibition. Whether maternal nutrient restriction (MNR) causes fetal hypoxia remains unclear. We used fetal liver from a baboon (*Papio* sp.) model of IUGR due to MNR (70% global diet of Control) and HepG2 cells as a model for human fetal hepatocytes and tested the hypothesis that mTOR-mediated IGFBP-1 hyperphosphorylation in response to hypoxia requires HIF-1α (hypoxia-inducible factor-1α) and REDD-1 (regulated in development and DNA-damage responses-1) signaling. Western blotting (n=6) and immunohistochemistry (n=3) using fetal liver indicated greater expression of HIF-1α, REDD-1 as well as erythropoietin and its receptor, and vascular endothelial growth-factor at GD120 (GD185 term) in MNR vs Control. Moreover, treatment of HepG2 cells with hypoxia (1% pO_2) (n=3) induced REDD-1, inhibited mTOR complex-1 (mTORC1) activity and increased IGFBP-1 secretion/phosphorylation (Ser101/Ser119/Ser169). HIF-1α inhibition by echinomycin

[*]Corresponding author: Dr. Madhulika B. Gupta, Children's Health Research Institute and Departments of Pediatrics and Biochemistry, University of Western Ontario, VRL Room A5-136 (WC), 800 Commissioners Road E., London, ON Canada N6C 2V5, Phone: (519)685-8500, Ext. 55099, Fax: (519) 685-8186, mbgupta@uwo.ca.

Author Contributions

TJ and MBG designed research; JK, BJ, KB, KN, CL, PWN, TJ, and MBG analyzed data; JK, BJ, KB, KN, and AWC performed research; TJ and MBG wrote the paper; JK wrote a draft of the paper; CL and PWN reviewed the paper and also contributed new reagents or analytic tools.

[#]Equal contribution

[$]Authorship attribution is equivalent

Conflict of Interest Statement

The authors have stated explicitly that there are no conflicts of interest in connection with this article.

or siRNA silencing prevented the hypoxia-mediated inhibition of mTORC1 and induction of IGFBP-1 secretion/phosphorylation. DMOG (dimethyloxaloylglycine) induced HIF-1α and also REDD-1 expression, inhibited mTORC1 and increased IGFBP-1 secretion/phosphorylation. Induction of HIF-1α (DMOG) and REDD-1 by Compound 3 inhibited mTORC1, increased IGFBP-1 secretion/ phosphorylation and protein kinase PKCα expression. Together, our data demonstrate that HIF-1α induction, increased REDD-1 expression and mTORC1 inhibition represent the mechanistic link between hypoxia and increased IGFBP-1 secretion/phosphorylation. We propose that maternal undernutrition limits fetal-oxygen delivery, as demonstrated by increased fetal liver expression of hypoxia-responsive proteins in baboon MNR. These findings have important implications for our understanding of the pathophysiology of restricted fetal growth.

Keywords

Fetal growth; Hypoxia-inducible Factor 1; Regulated in Development and DNA Damage Responses 1; Mechanistic Target of Rapamycin Complex 1; Fetal hypoxia; Non-human primate

Introduction

Intrauterine growth restriction (IUGR) affects ~5% of all newborns[1] and increases the risk of perinatal complications[1–3] and predisposes the infant to develop diabetes and cardiovascular disease in childhood and adult life[4–6].

Placental insufficiency due to, for example, a lack of normal increase in uteroplacental blood flow is the leading cause of IUGR in Western societies[7]. Placental insufficiency is associated with complex, coordinated, and highly regulated changes in placental signaling and nutrient transport ultimately leading to decreased delivery of oxygen and nutrients to the fetus, which is believed to cause a decreased growth rate. Many IUGR fetuses are hypoxemic in utero[8,9] and the link between decreased fetal oxygen availability and reduced fetal growth is illustrated by the well-established inverse correlation between altitude and birth weight in humans[10,11] and has been confirmed in animal experiments[12–14].

Whereas IUGR due to placental insufficiency is often associated with fetal hypoxia, the relationship between maternal undernutrition and fetal oxygenation is less well known. A well-established baboon model of maternal nutrient restriction (MNR) with 30% reduction in total food intake results in moderate (10–15%) decrease in fetal weight at gestational day (GD) 165 (Term GD185)[15,16]. Moderate MNR in baboons provides a valuable model to explore the impact of maternal undernutrition on the activity of hypoxia-responsive pathways in the fetus.

Hypoxia activates hypoxia-inducible factor 1 and 2 (HIF-1 and HIF-2), which are transcription factors that induce the expression of hypoxia-responsive genes[17,18]. Both HIF-1α and HIF-2α are predominantly expressed in the liver[17]. Low oxygen tension enhances the activity of HIF by stabilizing the HIF α-subunit, which triggers adaptive responses required for cell survival in hypoxic stress. HIF-1α and HIF-2α play distinct functions in mTOR signaling; HIF-2α activation is maintained for a longer duration but also

activates mTORC1, while HIF-1α requires severe hypoxia and is more sensitive to mTOR signaling[19,20].

The mechanistic target of rapamycin (mTOR) regulates cellular proliferation, metabolism and protein synthesis. mTOR exists as two functionally and structurally different complexes, mTORC1 and mTORC2. Activation of mTORC1 increases phosphorylation of 4E-BP1 (eukaryotic translation initiation factor 4E-binding protein 1) at Thr70 and P70S6K1 (ribosomal protein S6 kinase β-1) at Thr389, which promote gene transcription and protein translation. Hypoxia has been found to inactivate mTOR, decrease amino acid transport and decrease overall cellular metabolism[21].

HIF-1 activation in response to hypoxia induces REDD-1 (regulated in development and DNA damage responses)[22] expression, a well-known inhibitor of mTORC1 signaling. Furthermore, HIF-1 affects additional stress response pathways that influence development, metabolism, inflammation, circulatory and respiratory physiology. HIFs increase the synthesis of erythropoietin (EPO), promoting erythropoiesis, and vascular endothelial growth factor (VEGF) promoting vasculogenesis[23].

Hypoxia upregulates insulin-like growth factor (IGF) binding protein 1 (IGFBP-1), which modulates the bioavailability of IGF-1[24], a key regulator of fetal growth[25]. Phosphorylation of IGFBP-1 at Ser101/Ser119/Ser169 increases IGFBP-1 binding affinity for IGF-1, thus further reducing IGF-1 bioavailability and bioactivity[26]. We recently reported that hyperphosphorylation of IGFBP-1 and decreased IGF-1 bioactivity are associated with inhibition of mTOR signaling in the baboon fetal liver in response to MNR prior to IUGR onset[27]. Based on our studies in cultured HepG2 cells, inhibition of mTOR constitutes a key mechanistic link between hypoxia and increased secretion and phosphorylation of IGFBP-1[28]. However, the signaling pathways linking hypoxia to mTOR inhibition in fetal liver have not been identified.

Additionally, IGFBP-1 can be phosphorylated by multiple kinases[29,30]. Protein kinase-C (PKC), protein kinase-A, and casein kinase (CK2) have consensus sequences matching IGFBP-1 and may be responsible for phosphorylating IGFBP-1 at discrete sites during hypoxia. Regulation of hepatic IGFBP-1 synthesis by PKC in response to leucine deprivation has been reported previously[31,32] and we showed IGFBP-1 hyperphosphorylation in the same cells[32]. We have provided evidence that CK2 serves a key kinase responsible for phosphorylating IGFBP-1 during hypoxia in human endometrial stromal cells[33]. We have also shown CK2 expression and activity is activated in response to mTOR inhibition in HepG2 cells and in primary fetal baboon hepatocytes[26,34].

The purpose of this study was to test the overall *hypothesis* that mTOR-mediated IGFBP-1 hyperphosphorylation in response to hypoxia requires HIF-1α and REDD-1 signaling. We utilized liver from control and MNR baboon fetuses and performed western immunoblot and immunohistochemistry to determine the expression of hypoxia-responsive proteins (HIF-1, REDD-1, EPO, VEGF and EPO-R) at GD120 and GD165. Furthermore, we determined changes in mTORC1 activity, IGFBP-1 secretion/expression and site-specific phosphorylation, and protein-kinase expression in HepG2 cells following pharmacological

activation or inhibition of HIF-1α, siRNA mediated silencing of HIF-1α, and induction of REDD-1 in hypoxia or normoxia.

Materials and Methods

Baboon model of MNR

Baboons (*Papio* species) at the Southwest National Primate Research Center (San Antonio, TX, USA) were used. Details of housing and feeding regimens have been provided previously[35]. Following confirmation of pregnancy at 30 days of gestation, MNR was induced by feeding mothers 70% of total food (Purina Monkey Diet 5038) consumed by contemporaneous Controls. Fetuses were delivered and euthanized at gestational day (GD) 120 or GD165 (term 185 days), and following morphometric measurements, fetal liver tissue was collected and frozen in liquid nitrogen and stored at −80°C.

Cell culture

Human hepatoma (hepatocellular carcinoma) HepG2 cells (ATCC HB-8065, Manassas, VA, USA) with extensive similarity to primary human fetal hepatocytes[36,37] were used. Cells were cultured in Dulbecco's Modified Eagle Medium (DMEM) with F-12 (DMEM/F-12) supplemented with 10% fetal bovine serum (FBS) (Invitrogen) at 37°C in 20% O_2 and 5% CO_2 air as described previously[38]. Cells were plated in 6-well culture dishes and grown in 10% FBS at 75% confluency for 24 hours[39].

Protein extraction

Tissues from the left lobe of fetal liver at GD120 and GD165 from control and gestational age-matched MNR animals were stored frozen at −80°C. Fetal liver (~0.2 g each) were used for extraction of proteins using lysis buffer (Cell Signaling Technology, Danvers, MA, USA) with Protease Inhibitor Cocktail, Phosphatase Inhibitor Cocktail 2, and Phosphatase Inhibitor Cocktail 3 (Sigma-Aldrich, St. Louis, MO, USA) as described previously[26]. The homogenized samples were sonicated, centrifuged and the clear supernatant was collected and stored at −80°C.

Protein extraction from HepG2 cells was performed as described previously[26]. In brief, following treatment, cell media was collected, and cell lysates were prepared using lysis buffer (Cell Signaling Technology, Danvers, MA, USA). Cells were sonicated on ice and the supernatant was collected and stored at −80°C. Cell media and lysate were used for western blotting. Total protein concentration in liver tissue extracts and cell lysates was determined using Bradford assay.

SDS PAGE and Western blotting

Equal amounts of total protein (50 μg) from baboon fetal liver extracts were run on SDS-PAGE. Western blotting was performed to determine expression of total HIF-1α, REDD-1, EPO, VEGF, and EPO-R. Additionally, western blotting of HepG2 cell lysates was performed to determine expression of total HIF-1α, REDD-1, CK2 (α, α', and β), PKAα, and PKCα, and total expression and phosphorylation of 4E-BP1 at Thr70 and of P70S6K1 at Thr389 as functional readouts for mTORC1 signaling.

Equal volume of HepG2 cell media from control and treatments was loaded on SDS-PAGE and western blotting was performed to determine total expression of IGFBP-1 (10–30 μL aliquots) and IGFBP-1 phosphorylation (30–50 μL aliquots) at Ser101, Ser119, and Ser169. IGFBP-1 secretion and phosphorylation in cell media samples were normalized via equal plating of cells and equal loading of cell media, as performed previously[39].

For immunoblot analysis, 5% skim milk in Tris-buffered saline (TBS) plus 0.1% Tween-20 (TBST) was used for blocking for all antibodies except for IGFBP-1 antibody, where 5% bovine serum albumin (BSA) in TBS was used. All primary antibodies against total protein were obtained from Santa Cruz Biotechnology (Dallas, TX, USA) while primary antibodies targeting phosphorylated proteins and respective total proteins were from Cell Signaling Technology (Danvers, MA, USA), with the exception of the monoclonal IGFBP-1 (mAb 6303) antibody from Medix Biochemica (Kauniainen, Finland). Antibodies targeting CK2 were a gift from Dr. D.W. Litchfield (London, Canada). Custom IGFBP-1 polyclonal antibodies targeting Ser101, Ser119, and Ser169 were generated at YenZym (YenZym Antibodies, Brisbane, CA, USA), and have been previously validated extensively and used to detect phosphorylation of IGFBP-1[26,40]. Immunoblots were incubated in primary antibodies overnight at 4°C with subsequent incubation in secondary antibody for 1 hour at room temperature. Primary antibody dilutions for all were 1:1000 except for IGFBP-1 mAb that was 1:10000 and β-actin 1:3000. Secondary antibodies were peroxidase-labeled goat-anti mouse or goat-anti rabbit antibodies, 1:10000 (Bio-Rad Laboratories, Hercules, CA, USA). The membranes were exposed to enhanced chemiluminescence (ECL) reagents and imaged on a VersaDoc Imager (Bio-Rad Laboratories, Hercules, CA, USA). Band intensities were determined using densitometry and Image Lab software (Bio-Rad Laboratories, Hercules, CA, USA).

Immunohistochemistry (IHC)

Tissues from the left lobe of fetal liver at GD120 and GD165 from one control and gestational-age matched MNR tissue were fixed and sectioned (5 μm) on the same slide. Endogenous peroxidases were blocked using Bloxall™ (Vector Laboratories, Burlingame, CA, USA) and incubated with Background Sniper blocking solution (Biocare Medical, LLC., Pacheco, CA, USA). The sections were incubated overnight at 4°C with primary antibodies diluted with antibody diluent (Dako, Agilent Technologies, Santa Clara, CA, USA). Primary antibodies HIF-1α mouse mAb 1:500 (Abcam, Cambridge, UK), REDD-1 mouse mAb 1:500 (Santa Cruz Biotechnology, Dallas, TX, USA), EPO rabbit polyclonal 1:1500 (Thermo Fisher Scientific, Waltham, MA, USA), EPO-R rabbit polyclonal 1:350 (Santa Cruz Biotechnology, Dallas, TX, USA), and VEGF mouse mAb 1:350 (Novus Biologicals, Littleton, CO, USA) were used.

The tissue sections were incubated with secondary antibody, either anti-mouse or anti-rabbit horseradish peroxidase polymer complex (ImmPRESS® HRP Reagent Kit, Vector Laboratories, Burlingame, CA, USA), for 45 minutes and then treated with 3,3'-diaminobenzidine (DAB) substrate (Millipore Sigma, Burlington, MA, USA) for 4 minutes. The tissues were counter-stained with Modified Mayer's Haematoxylin (Thermo Fisher Scientific™ Richard-Allan Scientific™, Waltham, MA, USA), dehydrated through graded

ethanol series, cleared in xylene, and mounted with Permount (Thermo Fisher Scientific, Waltham, MA, USA).

Immunofluorescence (IF) microscopy

For HepG2 cell immunofluorescence (IF) microscopy, cells were plated on poly L-lysine coated glass coverslips and fixed after treatment with dimethyloxaloylglycine (500 μM) or Compound 3 (50 μM) (Sigma-Aldrich, St. Louis, MO, USA) using 4% paraformaldehyde. Cells were permeabilized using 0.25% TRITON X-100 in phosphate-buffered saline (PBS) × 10 minutes and blocked with Background Sniper (Biocare Medical, Pacheco, CA, USA). Primary antibodies diluted in Dako Diluent against phosphorylated IGFBP-1 at Ser101 (1:400), Ser119 (1:400), or Ser169 (1:200), polyclonal IGFBP-1 (1:2500, a kind gift from Dr. R. Baxter, Sydney, Australia), or PKCα (1:250) and incubated overnight at 4°C. The Alexa Fluor fluorescent secondary antibodies used were diluted in Dako diluent (1:400) anti-mouse 488 or anti-rabbit 568 (Thermo Fisher Scientific, Waltham, MA, USA) and incubated for 45 minutes at room temperature. Samples were counterstained with DAPI (1:300). The stained coverslips were mounted with ProLong Gold Antifade Mountant (Thermo Fisher Scientific, Waltham, MA, USA).

Image analysis

Multiple representative images from each baboon liver tissue or HepG2 cells were captured, broadly covering multiple randomly selected regions (n=10) of the liver tissue section or HepG2 fixed cells (n=3) to avoid bias and effectively represent the results.

For image analysis of liver tissue, Aperio Slide Scanner (Leica Microsystems, Wetzlar, Germany) was used. A macro was created using ImagePro Premier software (MediaCybernetics, Rockland, MD, USA) to highlight and quantify areas with the characteristic brown stain created by DAB to represent the localization of HIF-1α, REDD-1, EPO, EPO-R, or VEGF. Camera settings and exposure times were kept consistent throughout.

We used bright-field imaging at 40X magnification for liver tissue. The immunohistochemistry (IHC) images (n=3) of fetal parenchyma were analyzed quantitatively to determine percent area of staining of either HIF-1α, REDD-1, EPO, EPO-R, or VEGF for each of the images with this software. Data from multiple areas of the same Control tissues was averaged and analysed with averaged data from the MNR tissues.

Images for HepG2 cells were captured under a Zeiss AxioImager Z1 Microscope (Carl Zeiss Canada Ltd., North York, ON, Canada). Images were acquired with 63X magnification and visual assessment of fluorescently labeled proteins was performed for qualitative evaluation.

Parallel reaction monitoring mass spectrometry (PRM-MS)

We performed PRM-MS for the relative quantification of IGFBP-1 phosphorylation sites as well as phosphorylation sites for PKC and CK2 in control (Normoxia) and treated (DMOG and C3) HepG2 cell lysates. Immunoprecipitation (IP) was performed using monoclonal IGFBP-1 mAb 6303 as described previously[28]. Prior to immunoprecipitation, treatments

were validated for IGFBP-1 induction in cell lysate by Western blot (not shown). Novel single and/or dual IGFBP-1 phospho-sites and autophosphorylation sites for PKC and CK2 were all detected by targeted PRM-MS.

In brief, PRM-MS was performed using IP samples for in-solution digestions, the samples were first digested using endoproteinase Asp-N (Roche Diagnostics, Switzerland) and incubated overnight at 37°C, followed by a subsequent digestion using trypsin (Roche Diagnostics, Laval, QC, Canada) overnight at 37°C. Digests were then desalted by C18-Zip Tip and dried in a SpeedVac. After desalting and drying, peptides were reconstituted in 20 μL of 0.1% FA and loaded 4 μL onto a Thermo Easy-Spray analytical column (75 μm i.d. × 500 mm) C18 column. Peptides were separated on a 125 min (5–40% acetonitrile) gradient. Mass spectra were collected on a Q-Exactive hybrid quadrupole-Orbitrap mass spectrometer coupled to an Easy-nLC 1000 system (Thermo Fisher Scientific, Waltham, MA, USA) monitoring an isolation list (Supplemental Table S1). Relative changes in IGFBP-1 phosphorylation were determined by the total peak height of combined transitions. An internal IGFBP-1 peptide (NH2-ALPGEQQPLHALTR-COOH) was used to normalize all phosphorylated IGFBP-1 data. For peptides with two possible phosphorylation sites (dual), specific transitions were used to distinguish single site phosphorylation from each other (specifically, y14, b6 and b9 ions for pS169 and pS174; y12 and b15 ions for pS98 and pS101).

Additionally, PRM-MS analysis was performed using the co-immunoprecipitated (co-IP) samples for determining the expression and autophosphorylation of CK2 using CK2-specific peptides and peptide modifications (phosphorylation) and similarly for PKC. Several internal unmodified peptides for PKC and CK2 were used to each normalize respective phospho-peptide data for PKC and CK2.

HepG2 cell culture

Hypoxia treatments of HepG2 cells—HepG2 cells were cultured in normoxia or hypoxia as previously described[38,39]. In brief, cells were serum starved with 2% FBS and cultured normally at 37°C (20% O_2, 5% CO_2; incubator air, normoxia) or subjected to hypoxia. For hypoxia, cells were placed in a hypoxia chamber (Billups–Rothenburg, San Diego, CA, USA), which was flushed with a 1% O_2, 5% CO_2, balanced N_2 gas mixture (Linde Canada Ltd., Mississauga, ON, Canada) for 10 minutes to ensure a saturated hypoxic environment. The hypoxic chamber was then sealed, and cells were placed in a tissue-culture incubator at 37°C. Cells were cultured for 24 hours prior to collection of cell media and cell lysate.

Pharmacological treatment to alter HIF-1 and REDD-1 signaling in HepG2 cells—HepG2 cells grown to 75% confluency were serum-starved in 2% FBS overnight prior to treatment of cells with echinomycin (Sigma-Aldrich, St. Louis, MO, USA), dimethyloxaloylglycine (DMOG, Cayman Chemical Company, Ann Arbor, MI, USA) or Compound 3 (Sigma-Aldrich, St. Louis, MO, USA). Echinomycin is an inhibitor of HIF-1 activity, by blocking the binding of HIF-1 to DNA and preventing its activity as a transcription factor. DMOG increases the expression of HIF proteins by inhibiting their

breakdown. Compound 3 (C3) is an inducer of REDD-1. Dose and time dependency studies were performed to identify the optimal drug concentration (echinomycin 10 nM, DMOG 500 μM, and C3 50 μM) and time of incubation (24 hours) used in this study to maximize effects while minimizing cell death (not shown). Prior to treatment, media was changed to 2% FBS overnight (12–16 hours). Cells were subjected to inhibitor/activator treatments in normoxic or hypoxic conditions for 24 hours. Subsequently, cell media was collected and immediately stored at −80°C and cells were stored at −80°C prior to collection of lysate as described previously[28].

Small interfering RNA (siRNA) treatment to alter HIF-1α signaling in HepG2 cells—HepG2 cells were plated and allowed to grow to ~60% confluency. Cells were transfected with HIF-1α siRNA (5'-CCAGCCGCTGGAGACACAATCATAT-3'; 40 nM) (Ambion Cat. #4390824, Thermo Fisher Scientific, Waltham, MA, USA) using Dharmafect transfection reagent 4 (Thermo Fisher Scientific, Waltham, MA, USA) as described previously[26]. Immediately after transfection, cells were cultured for 48 hours in normoxia (20% O_2, 5% CO_2; incubator air) for maximal silencing. Cells were then serum-starved overnight and treated for 24 hours in either normoxia or hypoxia (in a hypoxia chamber as described). The efficiency of target silencing was determined at the protein level using western blot analysis.

Cell viability assay

We tested the effect of pharmacological agents and hypoxia treatments on HepG2 cell viability using the trypan blue exclusion assay, to ensure these treatments did not increase cell death (not shown). Cells were trypsinized following treatments and resuspended in 10% FBS media. 15 μL trypan blue was added to 15 μL of cell suspension (1:1). Cells were counted using a Bright-Line hemocytometer (Hausser Scientific, Horsam, PA, USA) to determine the measure of live/total cells, an indicator of cell viability. Cell counts were then used to equally plate cells prior to treatment.

Data presentation and statistics

Statistics were performed using Prism 7 (GraphPad Software Inc., CA, USA). For each protein quantified, the mean density of the control sample bands was assigned an arbitrary value of 1 and all individual densitometry values were expressed relative to this mean. To compare means, unpaired *t*-test or one-way ANOVA (analysis of variance) corrected) with Bonferroni's Multiple Comparisons Test were used. The results are expressed as Mean+SEM, with differences considered statistically significant at $p<0.05$.

Results

Fetal weight and liver weight in MNR unaffected at GD120 but decreased at GD165.

Morphometric measures, published in our previous papers[15,16,41], from MNR and control baboons at GD120 and GD165 are presented in Table 1. Fetal weights were unaffected by MNR at GD120 but reduced in MNR at GD165 (−13%, p=0.030). Similarly, relative fetal liver weight was unchanged at GD120 but reduced by 9% (p=0.047) at GD165, reflecting the onset of IUGR. The concentrations of some key essential amino acids, such as leucine,

isoleucine and phenylalanine, were decreased in fetal cord plasma at GD120 and/or GD165 in MNR animals, consistent with reduced nutrient availability.

Fetal liver expression of HIF-1α, REDD-1, EPO, EPO-R and VEGF is increased in MNR.

Using western blotting, we determined the changes in the expression of hypoxia-inducible proteins in MNR liver compared to Control. At GD120 but not at GD165, MNR induced HIF-1α (+115%, p=0.004, Fig. 1A) and REDD-1 (+114%, p=0.013, Fig. 1B). Fetal liver EPO expression was increased at both GD120 (+86%, p=0.002) and GD165 (+243%, p<0.001) (Fig. 1C) and so was EPO-R expression at GD120 (+45%, p=0.016) and GD165 (+173%, p=0.002) (Fig. 1D), as was VEGF at GD120 (+100%, p=0.002, Fig. 1E) and GD165 (+36%, p=0.030) in MNR liver.

Using immunohistochemistry (IHC), we determined HIF-1α, REDD-1, EPO, EPO-R and VEGF expression in Control and MNR fetal liver at GD120 and GD165 (Fig. 2). We qualitatively assessed IHC images for each protein (Fig. 2A–E). We quantified respective images for percent area stained representing each protein (Fig. 2i–v). Using brightfield imaging, we noted that at GD120, there are a high population of hematopoietic cells, and the hepatocytes are small, with little glycogen or lipid storage; however, at GD165, there are far fewer hematopoietic cells, and the hepatocytes contain large white spaces, suggesting increased glycogen or lipid presence which displaces organelles and protein signals to the edges of the cytoplasm. Due to these changing hepatic morphological features, we cannot readily compare staining of GD120 to GD165 tissue; GD165 tissue sections present decreased overall staining compared to GD120, but this may be potentially due to both developmental loss of hematopoietic cell population and altered hepatocyte staining localization (i.e. at the edges of cells vs throughout).

Consistent with western blot data (Fig. 1A), HIF-1α expression was increased (+38%, p=0.009) in MNR compared to Control at GD120, while there was no change at GD165 (Fig. 2i). HIF-1α expression appears most notable in hematopoietic cells compared to other areas of liver tissue at GD120 (Fig. 2A, **panel a-b**). REDD-1, EPO, EPO-R and VEGF were increased in MNR surrounding the central veins and generally throughout the liver tissue (Fig. 2B–E). Similarly, REDD-1 expression was increased in MNR compared to control at GD120 (+29%, p=0.037) but not significantly changed at GD165 (Fig. 2ii). EPO expression was markedly increased in MNR compared to control at GD120 (+66%, p=0.032) and GD165 (+167%, p=0.009) (Fig. 2iii). EPO-R expression is increased in MNR compared to control at GD120 (+132%, p=0.002) and at GD165 (+320%, p=0.038) (Fig. 2iv). Furthermore, VEGF expression is increased in MNR compared to Control at GD120 (+125%, p=0.011) and GD165 (+103%, p=0.035), (Fig. 2v).

Together our data show that expression of HIF-1α, REDD-1, VEGF, and EPO and EPO-R are all upregulated in the MNR fetal liver at GD120 compared to Controls. IHC data are consistent with our western blot data, showing that MNR increases the fetal liver expression of HIF-1α and several hypoxia-inducible proteins which play an important role in the hypoxia response.

HIF-1 inhibition in HepG2 cells prevents increased REDD-1 expression, mTORC1 inhibition and increased IGFBP-1 secretion and phosphorylation in response to hypoxia.

Considering that the expression of hypoxia-inducible proteins HIF-1α and REDD-1 is increased in baboon MNR fetal liver, we treated HepG2 cells with hypoxia alongside echinomycin to inhibit HIF-1 activity, to test the hypothesis that mTORC1-mediated IGFBP-1 hyperphosphorylation in response to hypoxia requires HIF-1α. Hypoxia induced REDD-1 expression (+233%, $p<0.001$) and inhibited mTORC1 activity (−63%, $p=0.014$) (Fig. 3A and B). However, inhibition of HIF-1 activity by echinomycin prevented hypoxia-induced increase in REDD-1 expression (Fig. 3A) and mTORC1 inhibition (Fig. 3B) in response to hypoxia. mTORC1 activity, as measured by phosphorylation of 4E-BP1 at Thr70 was markedly reduced in hypoxia, which was largely prevented in hypoxic HepG2 cells treated with echinomycin (Fig. 3B).

As expected, there was a significant increase in IGFBP-1 secretion (+809%, $p<0.001$) and phosphorylation at Ser101 (+24900%, $p<0.001$), Ser119 (+1900%, $p<0.001$) and Ser169 (+12400%, $p<0.001$) in hypoxia compared to normoxia, which was prevented by inhibition of HIF-1 activity by echinomycin (Fig. 3C–F), demonstrating a mechanistic role for HIF-1α upregulation in the increase in IGFBP-1 secretion and phosphorylation in hypoxia.

HIF-1α silencing in HepG2 cells prevents mTORC1 inhibition and increased IGFBP-1 secretion and phosphorylation in response to hypoxia.

In addition to inhibiting HIF-1 activity chemically using echinomycin, we further tested our hypothesis using a siRNA strategy to specifically inhibit HIF-1α expression in HepG2 cells cultured under hypoxic conditions. We first confirmed that the siRNA approach efficiently silenced HIF-1α (−49%, $p<0.001$, Fig. 4A) in HepG2 cells in hypoxia. Then, we used our approach to mechanistically confirm that HIF-1 activity is required for mTORC1 inhibition and increased IGFBP-1 secretion and phosphorylation in hypoxia.

Hypoxia inhibited mTORC1 activity as measured by phosphorylation of 4E-BP1 at Thr70 (−36%, $p=0.044$), but silencing of HIF-1α prevented inhibition of mTORC1 activity in hypoxia (Fig. 4B).

As expected, there was a significant increase in IGFBP-1 secretion (+100%, $p<0.001$, Fig. 5A) and phosphorylation at Ser101 (+79%, $p=0.014$, Fig. 5B), Ser119 (+76%, $p=0.028$, Fig. 5C) and Ser169 (+115%, $p=0.012$, Fig. 5D) in hypoxia compared to normoxia; silencing of HIF-1α in hypoxia prevented the hypoxia-mediated increase in IGFBP-1 secretion and phosphorylation at Ser101, Ser119, and Ser169 (Fig. 5A–D). These data indicate that HIF-1α regulates the increase in IGFBP-1 secretion and phosphorylation mediated via mTORC1 in hypoxia. Overall, these data confirm the mechanistic role of HIF-1α in the increase in IGFBP-1 secretion and phosphorylation mediated via mTORC1 in hypoxia.

HIF-1α induction in HepG2 cells in normoxia results in REDD-1 induction, mTORC1 inhibition, and increase in IGFBP-1 secretion and phosphorylation.

Further, to investigate and confirm that HIF-1α mediates the changes in IGFBP-1 secretion and phosphorylation in hypoxia, HepG2 cells were cultured under normoxia (used as a

control) or treated with hypoxia. Cells were also treated with DMOG, a small molecule HIF-1α inducer under normoxia conditions. Expression of REDD-1, mTORC1 activity, and site-specific IGFBP-1 phosphorylation were determined using western blot analysis.

HIF-1α expression was increased in hypoxia (+107%, p=0.001) and DMOG (+87%, p=0.008) treatments compared to the normoxia control (Fig. 6A). Western blot data further showed that lysate from hypoxia (+207%, p=0.015) and DMOG (+216%, p=0.013) treated cells had significantly induced REDD-1 expression (Fig. 6B). These data demonstrate that HIF-1α induction induces REDD-1 expression and inhibits mTORC1 activity in HepG2 cells both in response to hypoxia and DMOG treatments in a similar manner.

mTORC1 activity was inhibited, assessed by functional readouts: decreased phosphorylation of P70S6K1 at Thr389 (Fig. 6C) in hypoxia (−72%, p<0.001) and DMOG (−61%, p=0.001) and of phosphorylation of 4E-BP1 at Thr70 (Fig. 6D) in hypoxia (−52%, p=0.004) and DMOG (−29%, p=0.024) treatments, compared to normoxia controls. These data demonstrate that HIF-1α induction induces REDD-1 expression and inhibits mTORC1 activity in HepG2 cells in a similar manner in response to both hypoxia and DMOG.

We showed earlier (Fig. 3C–F) that hypoxia induces IGFBP-1 secretion and phosphorylation. Here, we found that IGFBP-1 secretion was induced by DMOG (+1522%, p<0.001, Fig. 7A). IGFBP-1 phosphorylation at Ser101 (+579%, p=0.002), Ser119 (+1548%, p<0.001), and Ser169 (+5748%, p<0.001) was significantly induced in HepG2 cell media after DMOG treatment of cells in normoxia (Fig. 7B–D), highly consistent with the response to hypoxia (Fig. 3C–F).

Together these data are consistent with the possibility that HIF-1α induction, increased REDD-1 expression and mTORC1 inhibition represent the mechanistic link between hypoxia and increased IGFBP-1 secretion and phosphorylation in HepG2 cells.

REDD-1 induction in HepG2 cells by C3 in normoxia results in mTORC1 inhibition and increased IGFBP-1 secretion and phosphorylation.

Further, to determine the role of REDD-1 in mTORC1-mediated IGFBP-1 secretion and phosphorylation in hypoxia, we specifically induced REDD-1 by treating HepG2 cells with C3 in normoxia. Western blot analysis showed that REDD-1 inducer C3 increased REDD-1 expression in HepG2 cells in normoxia (+62%, p=0.004, Fig. 8A). Importantly, REDD-1 induction by C3 did not affect HIF-1α expression (p=0.335), as HIF-1α is upstream of REDD-1 (Fig. 8B). C3 inhibited mTORC1 activity in HepG2 cells, as determined using relative decrease in phosphorylation of 4E-BP1 at Thr70 (−84%, p<0.001, Fig. 8C) and of P70S6K1 at Thr389 (−43%, p=0.042, Fig. 8D) as functional readouts of mTORC1.

Furthermore, IGFBP-1 secretion (+2433%, p<0.001) and phosphorylation at Ser101 (+1346%, p<0.001), Ser119 (+1580%, p<0.001), and Ser169 (+659%, p=0.001) were increased in response to REDD-1 induction in normoxia (Fig. 9A–D).

HIF-1α or REDD-1 induction in HepG2 cells in normoxia results in increased IGFBP-1 phosphorylation as determined by immunofluorescence.

As an additional alternative approach, we used qualitative immunofluorescence (IF) microscopy to determine IGFBP-1 phosphorylation at Ser101, Ser119 or Ser169 in DMOG or C3-treated HepG2 cells cultured under normoxia. Staining was assessed visually and compared to normoxia controls (Fig. 10, **panel a, d, g**). HIF-1α induction by DMOG increased IGFBP-1 phosphorylation at Ser101, Ser119 and Ser169 (Fig. 10, **panel b, e, h**), supporting western blot data shown earlier (Fig. 7B–D). Similarly, C3 also increased IGFBP-1 phosphorylation at Ser101/Ser119/Ser169 (Fig. 10, **panel c, f, i**) consistent with our western blot data (Fig. 9B–D).

Both DMOG and C3 treatments increased punctate staining of phosphorylated IGFBP-1 throughout HepG2 cells compared to Control, suggesting the possibility of distribution of IGFBP-1 in distinct areas within the cell. Although currently unclear, the staining for IGFBP-1 phosphorylation at Ser169 in C3-treated cells (Fig. 10, **panel i**) seems diffused throughout the cell rather than as prominent punctate staining detected in DMOG-treated HepG2 cells (Fig. 10, **panel h**).

HIF-1α or REDD-1 induction in HepG2 cells results in increased expression of protein kinases in normoxia.

Western bot analysis was performed for detection of potential changes in the expression of protein kinases in HepG2 cells following treatments with DMOG and C3 (Fig. 11). Cells treated with DMOG showed increased expression of PKCα (+45%, p=0.046, Fig. 11A) and CK2 catalytic subunits CK2α (+117% p=0.039, Fig. 11B) and CK2α' (+72%, p=0.029, Fig. 11C) compared to the normoxia control. REDD-1 induction by C3 also showed increases in PKCα (+81%, p=0.002, Fig. 11D) and CK2α (+49%, p=0.023, Fig. 11E) expression compared to Control. No change was detected in expression of PKAα or CK2β (not shown).

HIF-1α induction in HepG2 cells increased IGFBP-1 phosphorylation as determined by PRM-MS.

Using PRM-MS, we first determined changes in IGFBP-1 phosphorylation at new or novel sites with singly and dually phosphorylated residues in cell lysate immunoprecipitated with IGFBP-1 mAb. PRM-MS was performed on IGFBP-1 in pooled triplicate immunoprecipitated cell lysate samples from DMOG or C3-treated HepG2 cells. Immunoprecipitated cell lysate samples from DMOG treatment had significantly increased phosphorylation at the single residue Ser101 (+2515%, p=0.002, Fig. 12A). DMOG treatment also resulted in a significantly greater dual phosphorylation at Ser98+Ser101 (+1706%, p=0.024, Fig. 12A) relative to the normoxic control.

We further determined the expression of PKC and CK2 co-IP with IGFBP-1. We did not observe any significant increase in expression or autophosphorylation of PKC and CK2 at specific sites which are known to indicate PKC or CK2 activation. Both, the phosphorylation of PKC at Thr497 or at Ser657 (Fig. 12B), or CK2α at Tyr182 (Fig. 12C) remained unchanged in co-IP-IGFBP-1 from DMOG or C3 treated cells compared to normoxia.

HIF-1α or REDD-1 induction in HepG2 cells in normoxia results in increased expression of PKCα and IGFBP-1 in normoxia as determined by immunofluorescence (IF) microscopy.

As an additional approach to validate western blotting data, we next performed qualitative dual-IF staining for PKCα and IGFBP-1 expression in response to DMOG and C3 treatments in HepG2 cells cultured under normoxia. Our data obtained using visual assessment showed greater expression of PKCα (green staining) and IGFBP-1 (red staining) as a result of HIF-1α induction (by DMOG) or REDD-1 induction (by C3) (Fig. 13B–C) in HepG2 cells. DMOG-treated cells show apparent colocalization of PKCα/IGFBP-1 (overlapped red/green (orange)) staining (Fig. 13B). Although quantitative assessments for colocalization of IGFBP-1 with PKCα were not attempted, a zoomed-in panel shown below (Fig. 13B) highlights areas of possible orange/overlapped staining within these cells. PKCα (green) in DMOG-treated cells has diffuse green staining throughout the cells with only a few punctate bright green spots. On the other hand, the C3-treated cells showed bright green, distinct punctate staining throughout the cells (Fig. 13C) suggesting PKCα may be associated with organelles or vesicles as a result of REDD-1 induction in HepG2 cells under normoxic conditions.

Discussion

We show for the first time that MNR in pregnant non-human primates, which results in IUGR, causes increased expression of key hypoxia-inducible proteins, including HIF-1α, REDD-1, EPO, EPO-R, and VEGF in the fetal liver prior to the onset of restricted fetal growth. Our findings are consistent with the model that IUGR following MNR in non-human primates, similar to restricted fetal growth caused by placental insufficiency, is associated with fetal hypoxemia and liver hypoxia, which may directly contribute to the development of IUGR.

Using HepG2 cells we report that increased abundance of HIF-1α is mechanistically linked to increased REDD-1 expression, mTORC1 inhibition and increased IGFBP-1 secretion and phosphorylation in response to hypoxia. These observations are consistent with our previous studies demonstrating that mTOR inhibition is required for the increase in IGFBP-1 secretion and phosphorylation in response to hypoxia in HepG2 cells[28]. We thus propose that increased expression of HIF-1α in response to limitations in oxygen availability is mechanistically linked to restricted fetal growth, and is mediated by increased expression of REDD-1, resulting in inhibition of mTORC1 and subsequent increase in IGFBP-1 secretion and phosphorylation. Increased IGFBP-1 phosphorylation dramatically decreases the bioavailability of IGF-1, a key fetal growth factor (Fig. 14). We believe this work will further our understanding of the mechanisms underpinning IUGR.

Our data using fetal liver of MNR baboons show increased expression of several hypoxia-inducible proteins prior to IUGR development, suggesting that fetal liver hypoxia precedes the restriction of fetal growth. We found increased expression of HIF-1α at GD120 but not GD165. One possible explanation for this finding may be the reported transient nature of increased HIF-1α protein expression when hypoxia is prolonged[20]. Specifically, HIF-1α mRNA stability is reduced in chronic hypoxia which may result in normalization of HIF-1α protein levels despite maintained hypoxic stimuli and decreased HIF-1α protein degradation.

Negative feedback by REDD-1 expression may further reduce HIF-1α expression[42] in prolonged hypoxia. Another possibility is that the normal liver HIF-1α protein expression in late gestation MNR fetus reflects normalization of fetal oxygen availability. However, the elevated MNR fetal liver EPO, EPO-R and VEGF levels at GD165 does not support this hypothesis, and instead suggests the presence of some degree of liver hypoxia also in late gestation.

Using IHC, we also find that hematopoietic stem cells (HSCs) are present in the baboon fetal liver at GD120, but not at GD165. HSCs migrate to the bone marrow and thymus by the end of gestation where hematopoiesis is definitively established[43]. HIF-1α is a master regulator of metabolism and hypoxia, and plays a critical role in HSC metabolism by regulating the transcription of genes that are critical for hematopoietic activity in HSCs[44]. During hypoxia, HIF-1α levels are elevated in HSCs. Thus, another possible reason for no significant change in HIF-1α expression at GD165 in both western blotting and IHC may be due to the lack of presence of HSCs in the liver tissue extracts at GD165, compared to GD120.

VEGF and EPO are regulated by oxygen levels[45,46] and mice subjected to early fetal hypoxia developed IUGR and showed upregulation of HIF-1α and its target genes: VEGF, EPO and IGFBP-1[47]. VEGF and EPO expression levels were increased in baboon MNR fetal liver in this study. This suggest limitations in oxygen delivery in the MNR fetus, which activates signaling pathways promoting vasculogenesis, angiogenesis and erythropoiesis potentially as adaptation in hypoxia. VEGF levels have been reported to be increased in cord blood of full term human IUGR infants[48] and EPO levels in cord serum are negatively correlated with birth weight[49], possibly reflecting that IUGR is associated with some degree of hypoxemia[50]. Oxidative stress markers are elevated in many key tissues in human IUGR, including the liver and in cord plasma[51–53]. Similar to baboons, in a guinea pig model of IUGR due to MNR, fetal VEGF and EPO were elevated[54] suggesting that chronic hypoxia is a key signaling mechanism in IUGR.

In our study, we also observed limited glycogen and or lipid storage in fetal hepatocytes at GD120, however, at GD165, the hepatocytes contained larger white spaces suggesting increased glycogen and/or lipid presence. It has been shown previously[55] that liver glycogen increases progressively, but this increase is significantly lower in IUGR. Decreased glycogen storage or availability in the fetal liver may be another key contributing factor to IUGR not previously explored in our baboon fetal liver tissues.

Increased expression of IGFBP-1 is a marker for poor fetal nutrition[56] and lack of oxygenation[57]. Markedly increased IGFBP-1 abundance and phosphorylation in cord blood of human IUGR fetuses has been suggested to be linked to restricted fetal growth, mediated by decreased bioavailability of IGF-1[58]. A role for HIF-1 in the upregulation of IGFBP-1 mRNA and protein in hypoxia has been reported previously[58] because HIF-1 binds to a functional hypoxia regulation element (HRE) present in the IGFBP-1 gene[58]. The role of HIF-1 and the mechanisms involved in phosphorylation of IGFBP-1 at post translational level via HIF-1 has not been studied. Moreover, HIF-1α inhibits mTOR signaling[22] a finding replicated by the current study. We have previously reported that inhibition of mTOR activates CK2 activity and increases IGFBP-1 phosphorylation in the baboon fetal liver[26]. In

the present study, we found that the expression of HIF-1α and REDD-1 is increased in the fetal liver from MNR baboon. Together, our current observations provide a mechanistic link between HIF-1 activity, hypoxia, and increased IGFBP-1 phosphorylation.

Using western blotting, we found PKC and CK2 expression to be increased following induction of HIF-1α and REDD-1 in HepG2 cells in normoxia. While PKC Ser657 is a highly conserved site and mutations at this site have been linked to severe loss of catalytic activity[59], activation of PKC has been shown to be via phosphorylation of PKC at Thr497, which occurs within its activation loop and is a critical site for its activation[60]. On the other hand, Tyr182 is a well-established autophosphorylation site linked to CK2α activation[61].

Although we expected increased phosphorylation of these kinases based on the western blot data, phosphorylation of PKC at Thr497 or at Ser657 (Fig. 12B), or CK2α at Tyr182 (Fig. 12C) was unchanged in IGFBP-1 IP cell lysate from DMOG or C3 treated HepG2 cells compared to normoxic controls. Activation loop phosphorylation at PKC at Thr497 is dispensable for activity[62], however, C-domain phosphorylation of PKC at Ser657 is necessary for enzyme stability and catalytic competency[59,63]. Similar to PKC[64], CK2 is localized in the cytoplasm and intracellular organelles[65]. A possible explanation for no changes in CK2α at Tyr182 phosphorylation may be due to co-IP of additional known IGFBP-1-interacting CK2β subunits[34] which may abolish CK2α autophosphorylation[61]. These CK2 subunits are known to mediate IGFBP-1 phosphorylation in HepG2 cells[26].

Overall, we show that increased HIF-1α or REDD-1 alone in HepG2 cells inhibits mTORC1 signaling and causes IGFBP-1 hyperphosphorylation at Ser101, Ser119, Ser169 even in normoxia. Considering PKC consensus sites are Thr50 and Ser58, it is likely that PKC leads to IGFBP-1 phosphorylation at Ser101/Ser119/Ser169 indirectly. Although a quantitative assessment of images was not performed, it appears that HIF-1α induction potentially resulted in co-localization of PKC and IGFBP-1 as detected by dual-IF, while REDD-1 induction resulted in punctate IF staining of PKC (not detected in normoxia controls). These findings are consistent with the possibility that PKC is translocated in HepG2 cells. Indeed, the translocation of PKC to the plasma membrane is a hallmark of its activation[62] suggesting the possibility that PKC mediates IGFBP-1 phosphorylation indirectly in hypoxia via translocation.

CK2 consensus sequences match IGFBP-1 serine phospho-acceptor sites (Ser101, Ser119, Ser169); as a result, CK2 could directly phosphorylate IGFBP-1, though we were unable to determine if Tyr182-autophosphorylation (activation) of CK2 in DMOG/C3 was significant in our PRM-MS analyses. However, CK2 catalytic subunits (CK2α/α') have increased expression as a result of both HIF-1α and REDD-1 induction seen by western immunoblotting. The kinases mediating IGFBP-1 phosphorylation in HIF-1α or REDD-1 induction and the mechanisms involved remain to be identified.

In conclusion, our data suggest that limitations in fetal oxygen availability contributes to the restricted fetal growth in response to MNR. We propose that increased expression of HIF-1α in response to fetal hypoxia is mechanistically linked to restricted fetal growth. These changes are mediated by increased expression of REDD-1, resulting in inhibition

of mTOR and subsequent increase in IGFBP-1 secretion and phosphorylation. Increased IGFBP-1 phosphorylation decreases the bioavailability of IGF-1, a key fetal growth factor (Fig. 14).

Supplementary Material

Refer to Web version on PubMed Central for supplementary material.

Acknowledgements

We thank Dr. David W. Litchfield (Department of Biochemistry, University of Western Ontario, London, Canada) for the antibodies for protein kinase CK2 and Dr. Rob Baxter for the IGFBP-1 polyclonal antibody. We thank Biotron Integrated Microscopy (University of Western Ontario, London, Canada) for immunohistochemical and image acquisition analyses.

Funding

This work was supported by grants from the Natural Sciences and Engineering Research Council of Canada (NSERC) Discovery Grant (RGPIN to MBG), National Institute of Health (R03HD078313 to MBG and TJ), Program Project grant (P01HD021350 and R03HD093950 to PWN) and in part by Lawson Research Grant (F0609 to MBG). JK received Department of Pediatrics (UWO) Graduate Studentship and AWC received Children's Health Research Institute and Department of Pediatrics Graduate Studentship award (UWO).

Non-standard abbreviations:

IUGR	Intrauterine growth restriction
GD	Gestational day
HIF-1	Hypoxia-inducible factor 1
HIF-1α	alpha-subunit of HIF-1
REDD-1	Regulated in development and DNA damage responses 1
EPO	Erythropoietin
EPO-R	Erythropoietin receptor
VEGF	Vascular endothelial growth factor
mTORC1	Mechanistic target of rapamycin complex 1
IGF	Insulin-like growth factor
IGFBP-1	Insulin-like growth factor binding protein 1
4E-BP1	Eukaryotic translation initiation factor 4E-binding protein 1
P70S6K1	Ribosomal protein S6 kinase beta-1
PKA	Protein kinase A
PKC	Protein kinase C
CK2	Casein kinase

DMOG	Dimethyloxalylglycine
C3	Compound 3, REDD-1 inducer, 6-(1,3-Dioxo-6-(piperidin-1-yl)-1H-benzo[de]isoquinolin-2(3H)-yl)hexanoic acid

References

1. Romo A, Carceller R, Tobajas J. Intrauterine growth retardation (IUGR): epidemiology and etiology. Pediatr Endocrinol Rev PER. 2009;6Suppl 3:332–336. [PubMed: 19404231]
2. Dall'Asta A, Brunelli V, Prefumo F, Frusca T, Lees CC. Early onset fetal growth restriction. Matern Health Neonatol Perinatol. 2017;3:2. [PubMed: 28116113]
3. Pallotto EK, Kilbride HW. Perinatal outcome and later implications of intrauterine growth restriction. Clin Obstet Gynecol. 2006;49(2):257–269. [PubMed: 16721105]
4. Barker DJP, Godfrey KM, Gluckman PD, Harding JE, Owens JA, Robinson JS. Fetal nutrition and cardiovascular disease in adult life. The Lancet. 1993;341(8850):938–941.
5. Gluckman PD, Hanson MA, Cooper C, Thornburg KL. Effect of in utero and early-life conditions on adult health and disease. N Engl J Med. 2008;359(1):61–73. [PubMed: 18596274]
6. Gluckman PD, Hanson MA. Living with the past: evolution, development, and patterns of disease. Science. 2004;305(5691):1733–1736. [PubMed: 15375258]
7. Alexander BT. Placental insufficiency leads to development of hypertension in growth-restricted offspring. Hypertens Dallas Tex 1979. 2003;41(3):457–462.
8. Economides DL, Nicolaides KH. Blood glucose and oxygen tension levels in small-for-gestational-age fetuses. Am J Obstet Gynecol. 1989;160(2):385–389. [PubMed: 2916623]
9. Nicolaides KH, Economides DL, Soothill PW. Blood gases, pH, and lactate in appropriate- and small-for-gestational-age fetuses. Am J Obstet Gynecol. 1989;161(4):996–1001. [PubMed: 2801852]
10. Jensen GM, Moore LG. The effect of high altitude and other risk factors on birthweight: independent or interactive effects?Am J Public Health. 1997;87(6):1003–1007. [PubMed: 9224184]
11. Moore LG, Charles SM, Julian CG. Humans at high altitude: hypoxia and fetal growth. Respir Physiol Neurobiol. 2011;178(1):181–190. [PubMed: 21536153]
12. Aljunaidy MM, Morton JS, Cooke C-L, Davidge ST. Maternal vascular responses to hypoxia in a rat model of intrauterine growth restriction. Am J Physiol-Regul Integr Comp Physiol. 2016;311(6):R1068–R1075. [PubMed: 27760732]
13. Giussani DA, Salinas CE, Villena M, Blanco CE. The role of oxygen in prenatal growth: studies in the chick embryo. J Physiol. 2007;585(Pt 3):911–917. [PubMed: 17962335]
14. Parraguez VH, Mamani S, Cofré E, et al.Disturbances in Maternal Steroidogenesis and Appearance of Intrauterine Growth Retardation at High-Altitude Environments Are Established from Early Pregnancy. PLoS ONE. 2015;10(11).
15. Cox LA, Nijland MJ, Gilbert JS, et al.Effect of 30 per cent maternal nutrient restriction from 0.16 to 0.5 gestation on fetal baboon kidney gene expression. J Physiol. 2006;572(Pt 1):67–85. [PubMed: 16513668]
16. Schlabritz-Loutsevitch NE, Dudley CJ, Gomez JJ, et al.Metabolic adjustments to moderate maternal nutrient restriction. Br J Nutr. 2007;98(2):276–284. [PubMed: 17391566]
17. Hashimoto T, Shibasaki F. Hypoxia-inducible factor as an angiogenic master switch. Front Pediatr. 2015;3:33. [PubMed: 25964891]
18. Ratcliffe PJ. HIF-1 and HIF-2: working alone or together in hypoxia?J Clin Invest. 2007;117(4):862–865. [PubMed: 17404612]
19. Elorza A, Soro-Arnáiz I, Meléndez-Rodríguez F, et al.HIF2α Acts as an mTORC1 Activator through the Amino Acid Carrier SLC7A5. Mol Cell. 2012;48(5):681–691. [PubMed: 23103253]
20. Uchida T, Rossignol F, Matthay MA, et al.Prolonged hypoxia differentially regulates hypoxia-inducible factor (HIF)-1alpha and HIF-2alpha expression in lung epithelial cells: implication of natural antisense HIF-1alpha. J Biol Chem. 2004;279(15):14871–14878. [PubMed: 14744852]

21. Jansson T, Aye ILMH, Goberdhan DCI. The emerging role of mTORC1 signaling in placental nutrient-sensing. Placenta. 2012;33Suppl 2:e23–29. [PubMed: 22687819]
22. Brugarolas J, Lei K, Hurley RL, et al.Regulation of mTOR function in response to hypoxia by REDD1 and the TSC1/TSC2 tumor suppressor complex. Genes Dev. 2004;18(23):2893–2904. [PubMed: 15545625]
23. Haase VH. Regulation of erythropoiesis by hypoxia-inducible factors. Blood Rev. 2013;27(1):41–53. [PubMed: 23291219]
24. Ben Lagha N, Seurin D, Le Bouc Y, et al.Insulin-like growth factor binding protein (IGFBP-1) involvement in intrauterine growth retardation: study on IGFBP-1 overexpressing transgenic mice. Endocrinology. 2006;147(10):4730–4737. [PubMed: 16809446]
25. Hellström A, Ley D, Hansen-Pupp I, et al.Role of Insulinlike Growth Factor 1 in Fetal Development and in the Early Postnatal Life of Premature Infants. Am J Perinatol. 2016;33(11):1067–1071. [PubMed: 27603537]
26. Abu Shehab M, Damerill I, Shen T, et al.Liver mTOR Controls IGF-I Bioavailability by Regulation of Protein Kinase CK2 and IGFBP-1 Phosphorylation in Fetal Growth Restriction. Endocrinology. 2014;155(4):1327–1339. [PubMed: 24437487]
27. Kakadia JH, Jain BB, Biggar K, et al.Hyperphosphorylation of fetal liver IGFBP-1 precedes slowing of fetal growth in nutrient-restricted baboons and may be a mechanism underlying IUGR. Am J Physiol Endocrinol Metab. 2020;319(3):E614–E628. [PubMed: 32744097]
28. Damerill I, Biggar KK, Abu Shehab M, Li SS-C, Jansson T, Gupta MB. Hypoxia Increases IGFBP-1 Phosphorylation Mediated by mTOR Inhibition. Mol Endocrinol. 2016;30(2):201–216. [PubMed: 26714229]
29. Ankrapp DP, Jones JI, Clemmons DR. Characterization of insulin-like growth factor binding protein-1 kinases from human hepatoma cells. J Cell Biochem. 1996;60(3):387–399. [PubMed: 8867814]
30. Frost RA, Tseng L. Insulin-like growth factor-binding protein-1 is phosphorylated by cultured human endometrial stromal cells and multiple protein kinases in vitro. J Biol Chem. 1991;266(27):18082–18088. [PubMed: 1655736]
31. Lee PD, Abdel-Maguid LS, Snuggs MB. Role of protein kinase-C in regulation of insulin-like growth factor-binding protein-1 production by HepG2 cells. J Clin Endocrinol Metab. 1992;75(2):459–464. [PubMed: 1379255]
32. Malkani N, Biggar K, Shehab MA, Li S, Jansson T, Gupta MB. Increased IGFBP-1 phosphorylation in response to leucine deprivation is mediated by CK2 and PKC. Mol Cell Endocrinol. 2016;425:48–60. [PubMed: 26733150]
33. Abu Shehab M, Biggar K, Kakadia JH, et al.Inhibition of decidual IGF-1 signaling in response to hypoxia and leucine deprivation is mediated by mTOR and AAR pathways and increased IGFBP-1 phosphorylation. Mol Cell Endocrinol. 2020;512:110865. [PubMed: 32502935]
34. Singal SS, Nygard K, Dhruv MR, et al.Co-Localization of Insulin-Like Growth Factor Binding Protein-1, Casein Kinase-2β, and Mechanistic Target of Rapamycin in Human Hepatocellular Carcinoma Cells as Demonstrated by Dual Immunofluorescence and in Situ Proximity Ligation Assay. Am J Pathol. 2018;188(1):111–124. [PubMed: 29037858]
35. Li C, Schlabritz-Loutsevitch NE, Hubbard GB, et al.Effects of maternal global nutrient restriction on fetal baboon hepatic insulin-like growth factor system genes and gene products. Endocrinology. 2009;150(10):4634–4642. [PubMed: 19574404]
36. Kelly JH, Darlington GJ. Modulation of the liver specific phenotype in the human hepatoblastoma line Hep G2. Vitro Cell Dev Biol J Tissue Cult Assoc. 1989;25(2):217–222.
37. Wilkening S, Stahl F, Bader A. Comparison of primary human hepatocytes and hepatoma cell line Hepg2 with regard to their biotransformation properties. Drug Metab Dispos Biol Fate Chem. 2003;31(8):1035–1042. [PubMed: 12867492]
38. Seferovic MD, Chen S, Pinto DM, Gupta MB. Altered Liver Secretion of Vascular Regulatory Proteins in Hypoxic Pregnancies Stimulate Angiogenesis in vitro. J Proteome Res. 2011;10(4):1495–1504. [PubMed: 21319863]

39. Seferovic MD, Ali R, Kamei H, et al.Hypoxia and Leucine Deprivation Induce Human Insulin-Like Growth Factor Binding Protein-1 Hyperphosphorylation and Increase Its Biological Activity. Endocrinology. 2009;150(1):220–231. [PubMed: 18772238]
40. Abu Shehab M, Iosef C, Wildgruber R, Sardana G, Gupta MB. Phosphorylation of IGFBP-1 at discrete sites elicits variable effects on IGF-I receptor autophosphorylation. Endocrinology. 2013;154(3):1130–1143. [PubMed: 23354097]
41. Kavitha JV, Rosario FJ, Nijland MJ, et al.Down-regulation of placental mTOR, insulin/IGF-I signaling, and nutrient transporters in response to maternal nutrient restriction in the baboon. FASEB J. 2014;28(3):1294–1305. [PubMed: 24334703]
42. Horak P, Crawford AR, Vadysirisack DD, et al.Negative feedback control of HIF-1 through REDD1-regulated ROS suppresses tumorigenesis. Proc Natl Acad Sci U S A. 2010;107(10):4675–4680. [PubMed: 20176937]
43. Jagannathan-Bogdan M, Zon LI. Hematopoiesis. Development. 2013;140(12):2463–2467. [PubMed: 23715539]
44. Zhang CC, Sadek HA. Hypoxia and Metabolic Properties of Hematopoietic Stem Cells. Antioxid Redox Signal. 2014;20(12):1891–1901. [PubMed: 23621582]
45. Ahmed A, Dunk C, Ahmad S, Khaliq A. Regulation of placental vascular endothelial growth factor (VEGF) and placenta growth factor (PIGF) and soluble Flt-1 by oxygen--a review. Placenta. 2000;21Suppl A:S16–24. [PubMed: 10831117]
46. Maiese K, Chong ZZ, Hou J, Shang YC. Erythropoietin and Oxidative Stress. Curr Neurovasc Res. 2008;5(2):125–142. [PubMed: 18473829]
47. Ream M, Ray AM, Chandra R, Chikaraishi DM. Early fetal hypoxia leads to growth restriction and myocardial thinning. Am J Physiol Regul Integr Comp Physiol. 2008;295(2):R583–595. [PubMed: 18509101]
48. Malamitsi-Puchner A, Boutsikou T, Economou E, et al.Vascular Endothelial Growth Factor and Placenta Growth Factor in Intrauterine Growth-Restricted Fetuses and Neonates. Mediators Inflamm. 2005;2005(5):293–297. [PubMed: 16258196]
49. Ostlund E, Lindholm H, Hemsen A, Fried G. Fetal erythropoietin and endothelin-1: relation to hypoxia and intrauterine growth retardation. Acta Obstet Gynecol Scand. 2000;79(4):276–282. [PubMed: 10746842]
50. Teramo KA, Widness JA. Increased Fetal Plasma and Amniotic Fluid Erythropoietin Concentrations: Markers of Intrauterine Hypoxia. Neonatology. 2009;95(2):105–116. [PubMed: 18776724]
51. Guvendag Guven ES, Karcaaltincaba D, Kandemir O, Kiykac S, Mentese A. Cord blood oxidative stress markers correlate with umbilical artery pulsatility in fetal growth restriction. J Matern-Fetal Neonatal Med Off J Eur Assoc Perinat Med Fed Asia Ocean Perinat Soc Int Soc Perinat Obstet. 2013;26(6):576–580.
52. Potdar N, Singh R, Mistry V, et al.First-trimester increase in oxidative stress and risk of small-for-gestational-age fetus. BJOG Int J Obstet Gynaecol. 2009;116(5):637–642.
53. Rashid CS, Bansal A, Simmons RA. Oxidative Stress, Intrauterine Growth Restriction, and Developmental Programming of Type 2 Diabetes. Physiol Bethesda Md. 2018;33(5):348–359.
54. Elias AA, Maki Y, Matushewski B, Nygard K, Regnault TRH, Richardson BS. Maternal nutrient restriction in guinea pigs leads to fetal growth restriction with evidence for chronic hypoxia. Pediatr Res. 2017;82(1):141–147. [PubMed: 28376077]
55. Cheng KM. Hepatic glycogen metabolism in normal developing and intrauterine growth-retarded rat fetuses. Nihon Sanka Fujinka Gakkai Zasshi. 1988;40(6):781–788. [PubMed: 3134501]
56. Chard TInsulin-like growth factors and their binding proteins in normal and abnormal human fetal growth. Growth Regul. 1994;4(3):91–100. [PubMed: 7532055]
57. Tapanainen PJ, Bang P, Wilson K, Unterman TG, Vreman HJ, Rosenfeld RG. Maternal hypoxia as a model for intrauterine growth retardation: effects on insulin-like growth factors and their binding proteins. Pediatr Res. 1994;36(2):152–158. [PubMed: 7526325]
58. Tazuke SI, Mazure NM, Sugawara J, et al.Hypoxia stimulates insulin-like growth factor binding protein 1 (IGFBP-1) gene expression in HepG2 cells: A possible model for IGFBP-1 expression in fetal hypoxia. Proc Natl Acad Sci U S A. 1998;95(17):10188–10193. [PubMed: 9707622]

59. Gysin S, Imber R. Replacement of Ser657 of protein kinase C-alpha by alanine leads to premature down regulation after phorbol-ester-induced translocation to the membrane. Eur J Biochem. 1996;240(3):747–750. [PubMed: 8856079]

60. Cazaubon S, Bornancin F, Parker PJ. Threonine-497 is a critical site for permissive activation of protein kinase C alpha. Biochem J. 1994;301 (Pt 2):443–448. [PubMed: 8042986]

61. Donella-Deana A, Cesaro L, Sarno S, Brunati AM, Ruzzene M, Pinna LA. Autocatalytic tyrosine-phosphorylation of protein kinase CK2 alpha and alpha' subunits: implication of Tyr182. Biochem J. 2001;357(Pt 2):563–567. [PubMed: 11439109]

62. Gould CM, Newton AC. The Life and Death of Protein Kinase C. Curr Drug Targets. 2008;9(8):614–625. [PubMed: 18691009]

63. Bornancin F, Parker PJ. Phosphorylation of protein kinase C-alpha on serine 657 controls the accumulation of active enzyme and contributes to its phosphatase-resistant state. J Biol Chem. 1997;272(6):3544–3549. [PubMed: 9013603]

64. Luria A, Tennenbaum T, Sun QY, Rubinstein S, Breitbart H. Differential localization of conventional protein kinase C isoforms during mouse oocyte development. Biol Reprod. 2000;62(6):1564–1570. [PubMed: 10819756]

65. Faust M, Montenarh M. Subcellular localization of protein kinase CK2. A key to its function?Cell Tissue Res. 2000;301(3):329–340. [PubMed: 10994779]

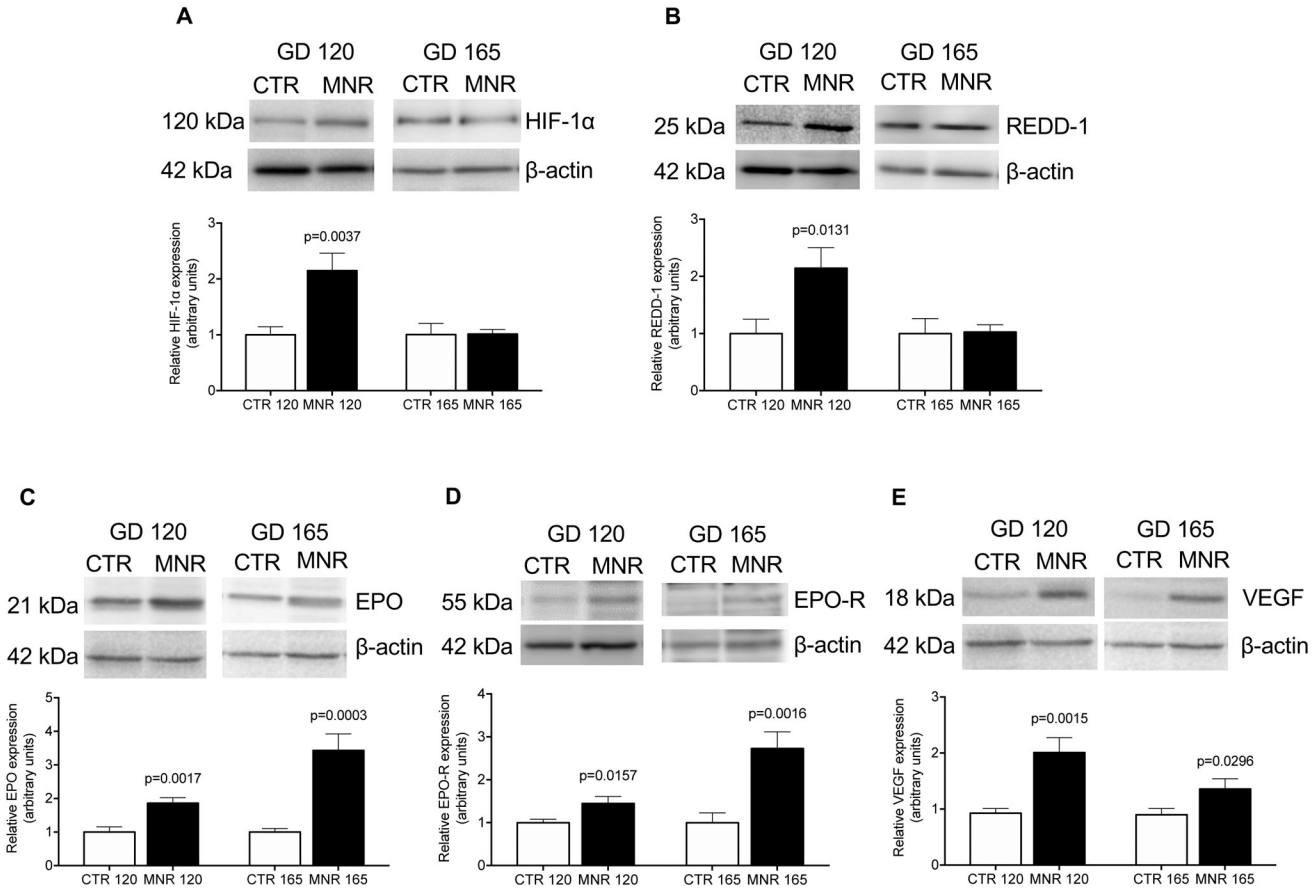

Figure 1. MNR is associated with increased expression of hypoxia-inducible proteins in baboon fetal liver prior to IUGR onset.

A representative western blot of HIF-1α (**A**), REDD-1 (**B**), EPO (**C**), EPO-R (**D**), and VEGF (**E**) expression in baboon fetal liver in Control (CTR) (n=6) and MNR (n=6) at GD120 and GD165.

CTR was assigned a value of 1 (arbitrary units) and MNR was normalized to CTR for comparisons between groups. Equal loading (50 μg) was performed, β-actin is the loading control. Values (n=6 each) are presented as Mean+SEM, unpaired *t*-test, $p<0.05$ is considered significant.

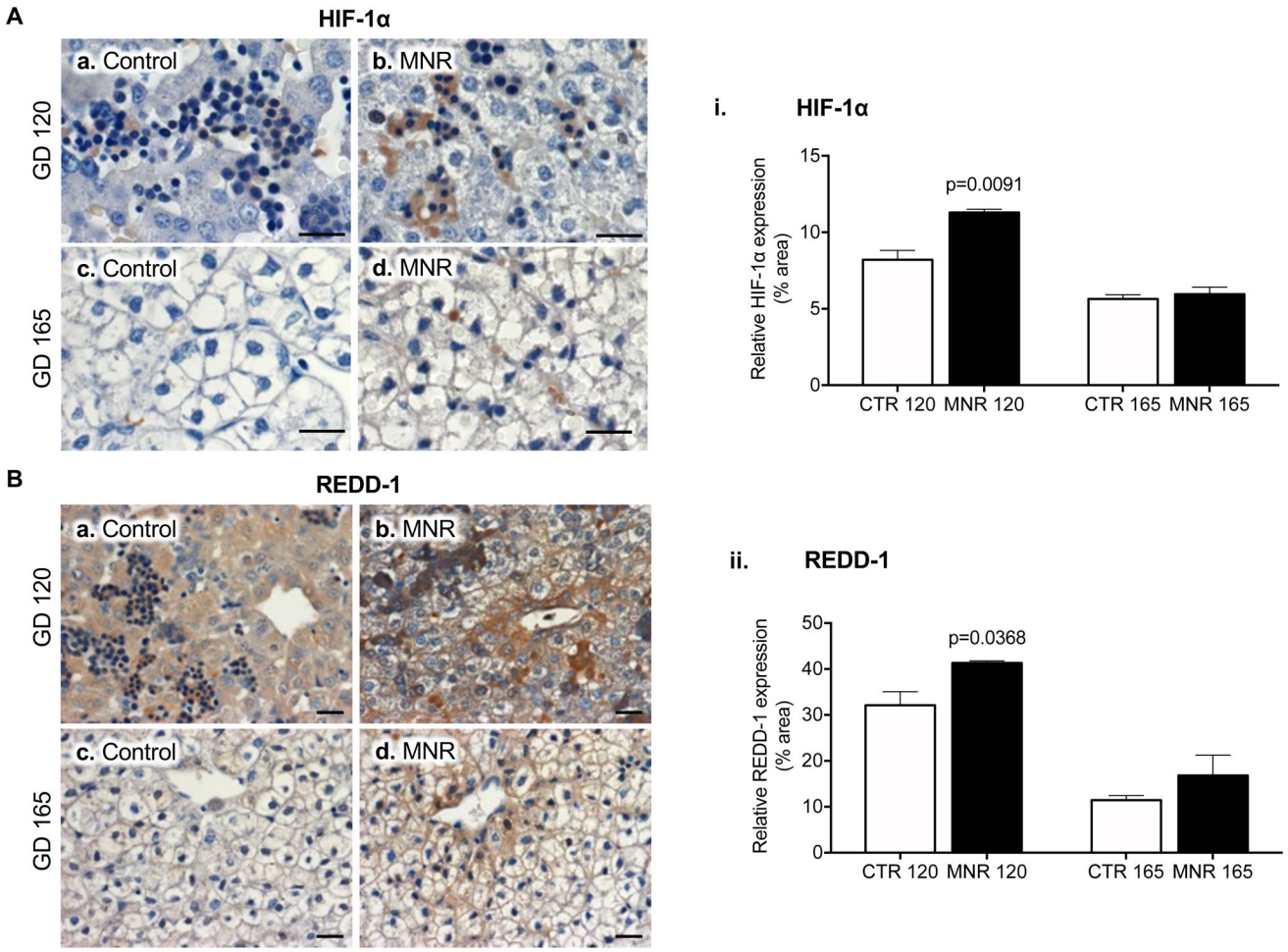

Figure 2. MNR is associated with increased expression of hypoxia-inducible proteins in fetal liver prior to IUGR onset as determined with immunohistochemistry.

Representative immunohistochemistry (IHC) images for HIF-1α (**A**), REDD-1 (**B**), EPO (**C**), EPO-R (**D**), and VEGF (**E**) expression in the parenchyma (brown staining) of left liver lobules from GD120 Control (CTR) (**a**) and MNR (**b**) and from GD165 CTR (**c**) and MNR (**d**). Liver tissue sections (n=3 each) were fixed on the same slide and stained with respective primary antibody. Hematoxylin nuclear counterstain is shown in blue, while positive signals are brown. 40x magnification is used (original scale bars, 50 μm).

The bar graphs summarize the quantification of IHC images (n=3 each) for HIF-1α (**i**), REDD-1 (**ii**), EPO (**iii**), EPO-R (**iv**), and VEGF (**v**) expression. IHC images were quantified using ImagePro software. Data is represented as % area stained in CTR vs MNR parenchyma at GD120 and GD165 respectively. Values (n=3 each) are displayed as Mean+SEM, unpaired *t*-test, $p<0.05$ is considered significant.

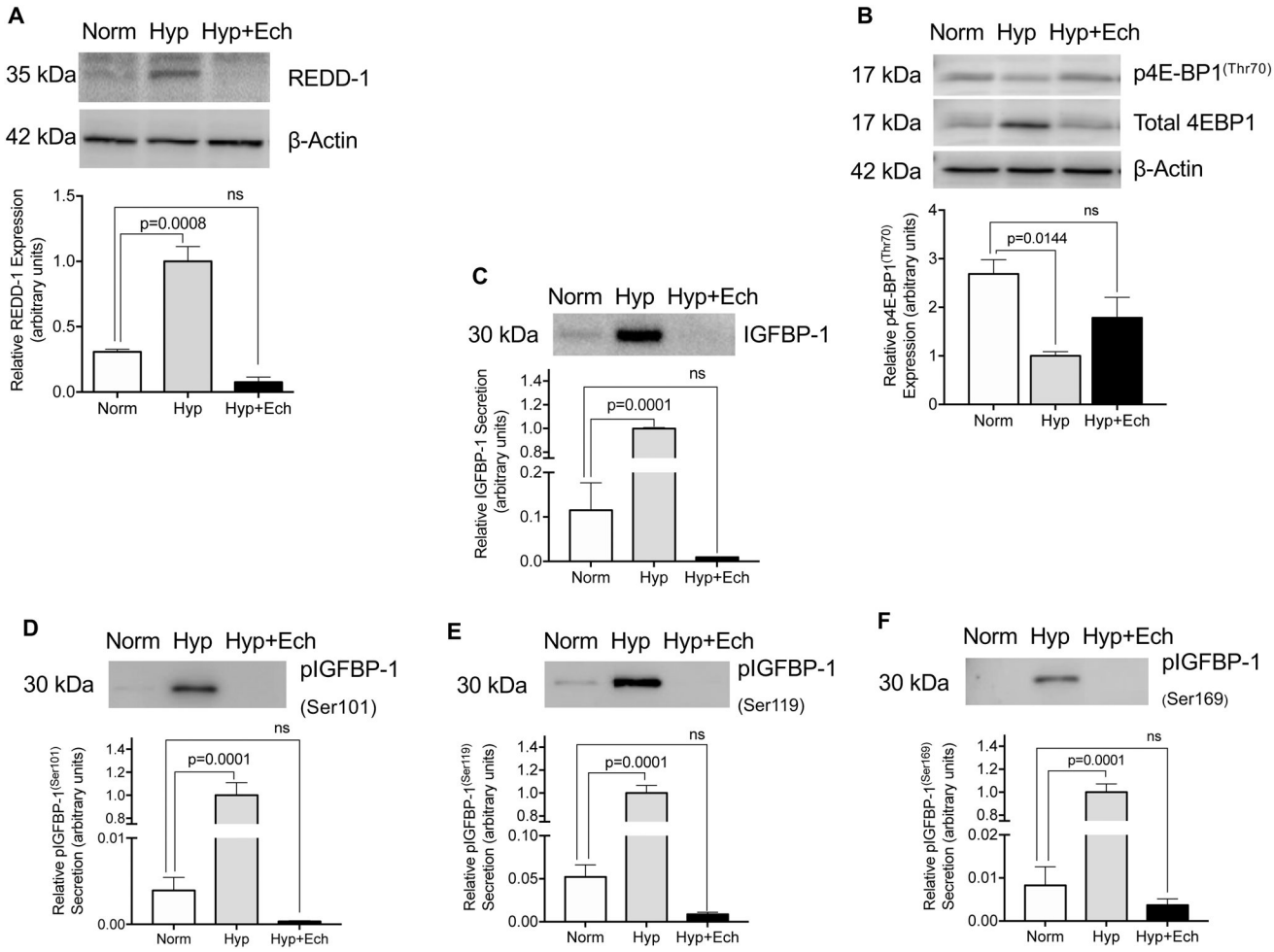

Figure 3. Echinomycin prevents hypoxia induced increase in REDD-1 expression, mTORC1 inhibition and IGFBP-1 secretion and phosphorylation in HepG2 cells

A representative western blot of REDD-1 (**A**) and mTORC1 functional readout 4E-BP1 phosphorylation at Thr70 (**B**) in cell lysate of HepG2 cells in normoxia (Norm), hypoxia (Hyp), or hypoxia+echinomycin (Hyp+Ech) treatments. Equal loading (50 μg) was performed. The bar graphs summarize the western blot data of protein expression with β-actin as the loading control.

A representative western blot of IGFBP-1 secreted by Norm, Hyp, or Hyp+Ech treated HepG2 cells (**C**). Equal aliquots of cell media (10 μL) used as loading controls. The bar graphs summarize the western blot data of proteins secreted in cell media.

Representative western blots of IGFBP-1 phosphorylation at Ser101 (**D**), Ser119 (**E**) and Ser169 (**F**) in cell media of Norm, Hyp, or Hyp+Ech treated HepG2 cells. Equal aliquots of cell media (30 μL) used as loading controls. The bar graphs summarize the western blot data of proteins secreted in cell media.

Hyp was assigned a value of 1 (arbitrary units) and Norm and Hyp+Ech treatment groups were normalized to the hypoxia group to facilitate comparisons between groups. Values (n=3 each) are displayed as Mean+SEM; One-way analysis of variance, corrected with Bonferroni's Multiple Comparisons test, $p<0.05$ considered significant.

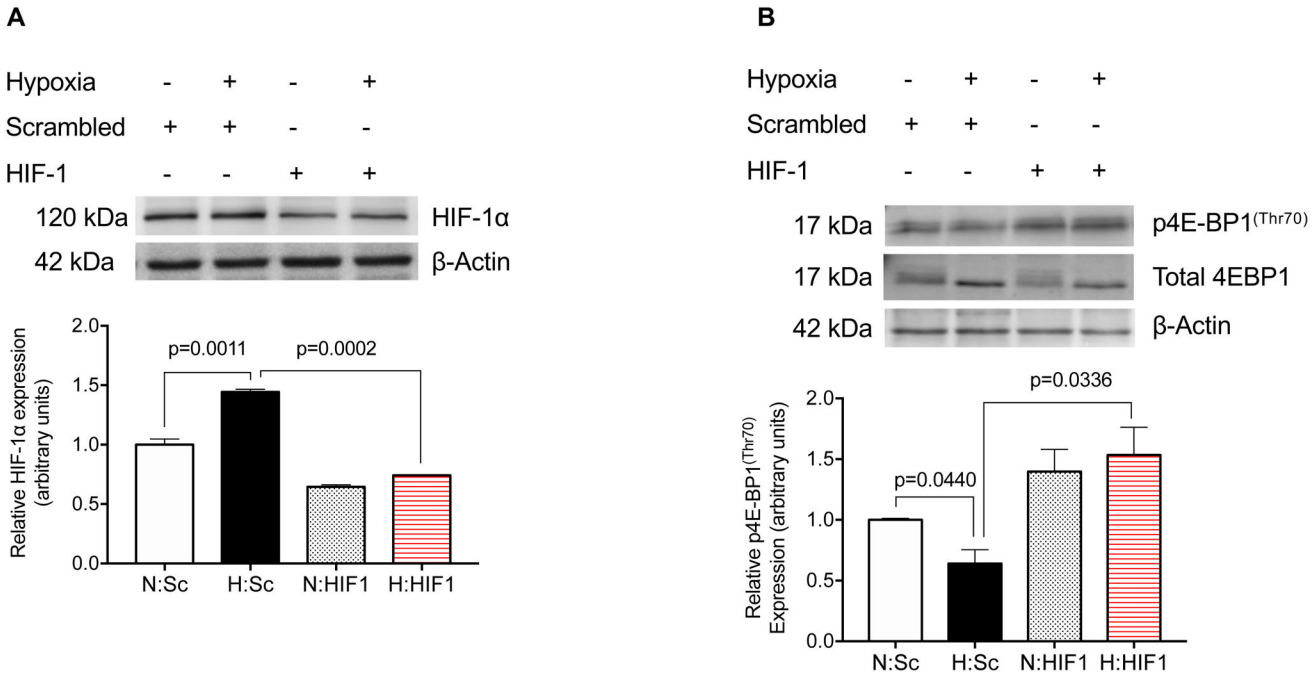

Figure 4. HIF-1α silencing by siRNA prevents hypoxia-induced increased HIF-1α expression and mTORC1 inhibition in HepG2 cells.

A representative western blot of HIF-1α (**A**) and mTORC1 functional readout 4E-BP1 phosphorylation at Thr70 (**B**) in cell lysate of HepG2 cells treated with scrambled or HIF-1α 6and then additionally cultured in normoxia or hypoxia. Equal loading (50 μg) was performed. The bar graphs summarize the western blot data of protein expression with β-actin as the loading control.

The normoxia:scrambled siRNA (N:Sc) group was assigned a value of 1 (arbitrary units) and treatment groups were normalized to this group to facilitate comparisons between groups. Values (n=3 each) are displayed as Mean+SEM; One-way analysis of variance, corrected with Bonferroni's Multiple Comparisons test, $p<0.05$ considered significant.

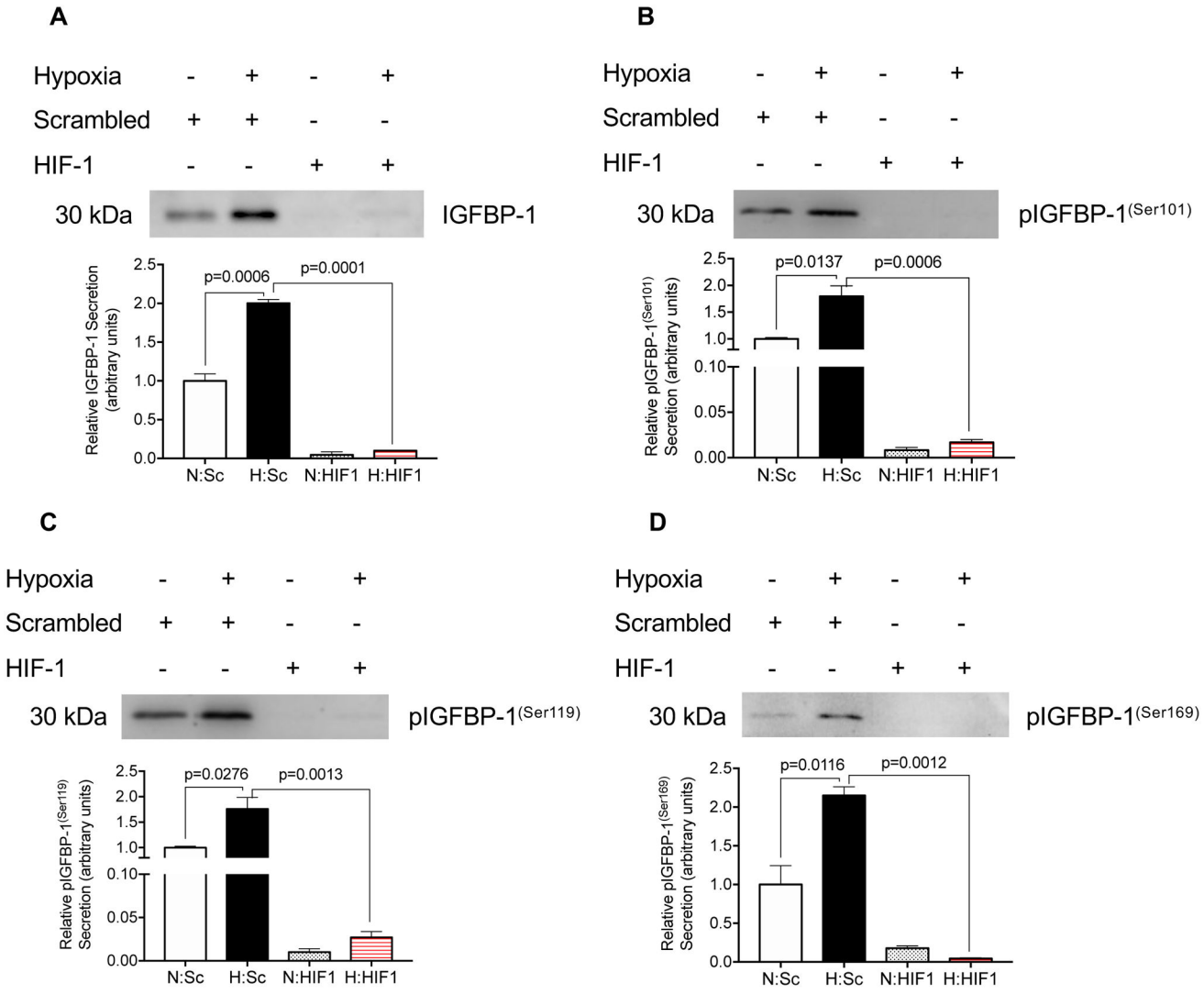

Figure 5. HIF-1α silencing by siRNA prevents hypoxia-induced increase in IGFBP-1 secretion and phosphorylation in HepG2 cells.

A representative western blot of IGFBP-1 (**A**) secreted by HepG2 cells treated with scrambled (Sc) or HIF-1α (HIF) siRNA and cultured in normoxia (N) or hypoxia (H). Equal aliquots of cell media (30 μL) used as loading controls. The bar graphs summarize the western blot data of proteins secreted in cell media.

Representative western blots of IGFBP-1 phosphorylation at Ser101 (**B**), Ser119 (**C**) and Ser169 (**D**) secreted by HepG2 cells treated with scrambled (Sc) or HIF-1α (HIF) siRNA and cultured in normoxia (N) or hypoxia (H). Equal aliquots of cell media (50 μL) used as loading controls. The bar graphs summarize the western blot data of proteins secreted in cell media.

The normoxia:scrambled siRNA (N:Sc) group was assigned a value of 1 (arbitrary units) and treatment groups were normalized to this group to facilitate comparisons between groups. Values (n=3 each) are displayed as Mean+SEM; One-way analysis of variance, corrected with Bonferroni's Multiple Comparisons test, $p<0.05$ considered significant.

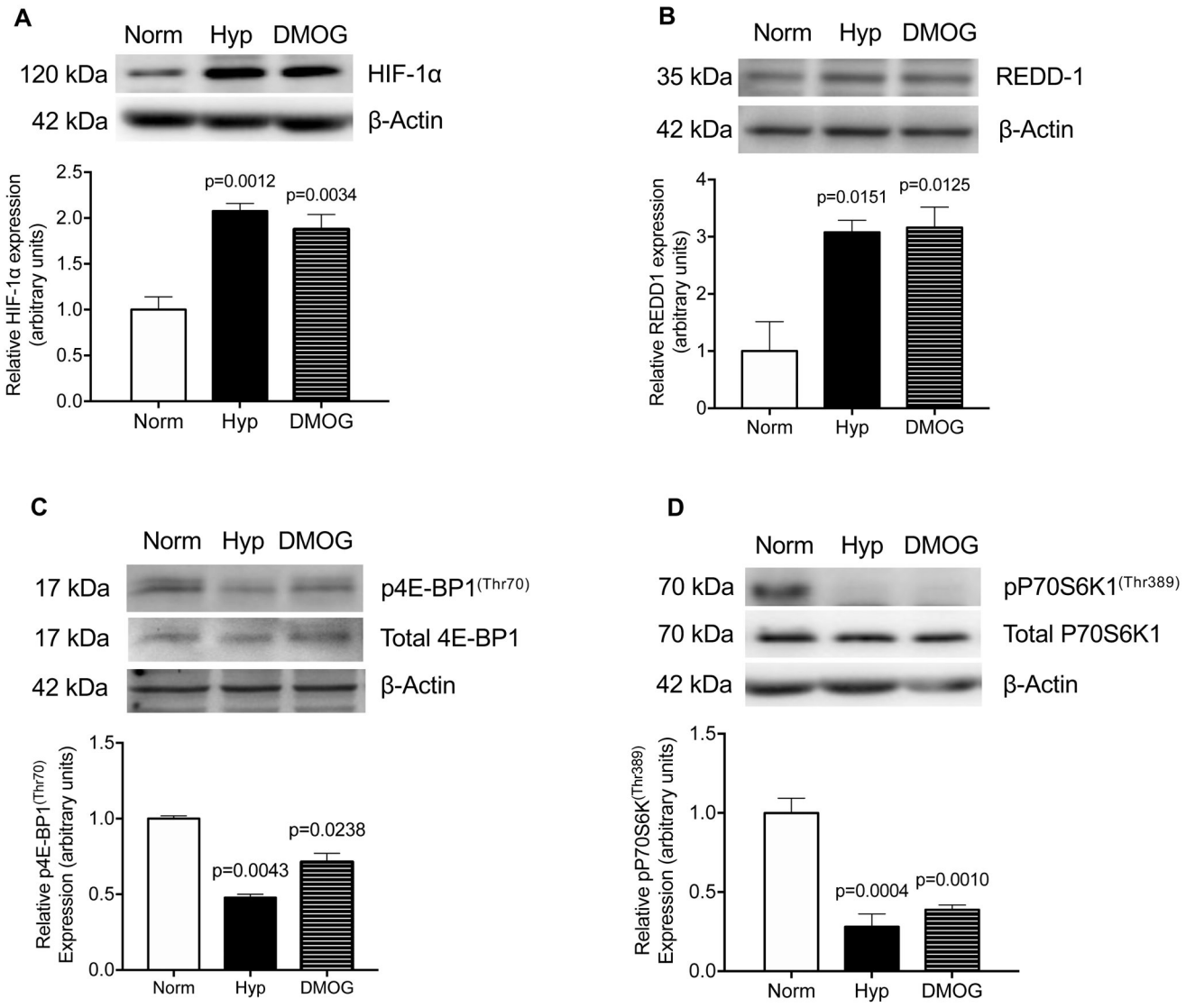

Figure 6. Hypoxia and DMOG treatments induce expression of HIF-1α and REDD-1 and inhibit mTORC1 activity in HepG2 cells in normoxia.

A representative western blot of HIF-1α (**A**) and REDD-1 (**B**) in cell lysate from HepG2 cells cultured for in normoxia (Norm), hypoxia (Hyp), or normoxia with DMOG (DMOG). Equal loading (50 μg) was performed. The bar graphs summarize the western blot data of protein expression with β-actin as the loading control.

A representative western blot of mTORC1 functional readouts 4E-BP1 phosphorylation at Thr70 (**C**) and P70S6K1 phosphorylation at Thr389 (**D**) in cell lysate from Norm, Hyp or DMOG-treated HepG2 cells. Equal loading (50 μg) was performed. The bar graphs summarize the western blot data as the ratio of phosphorylated to total protein with β-actin as the loading control.

Control Norm was assigned a value of 1 (arbitrary units) and treatment groups (Hyp and DMOG) were normalized to Norm to facilitate comparisons between groups. Values (n=3 each) are displayed as Mean+SEM; One-way analysis of variance corrected with Bonferroni's Multiple Comparisons test, $p<0.05$ considered significant.

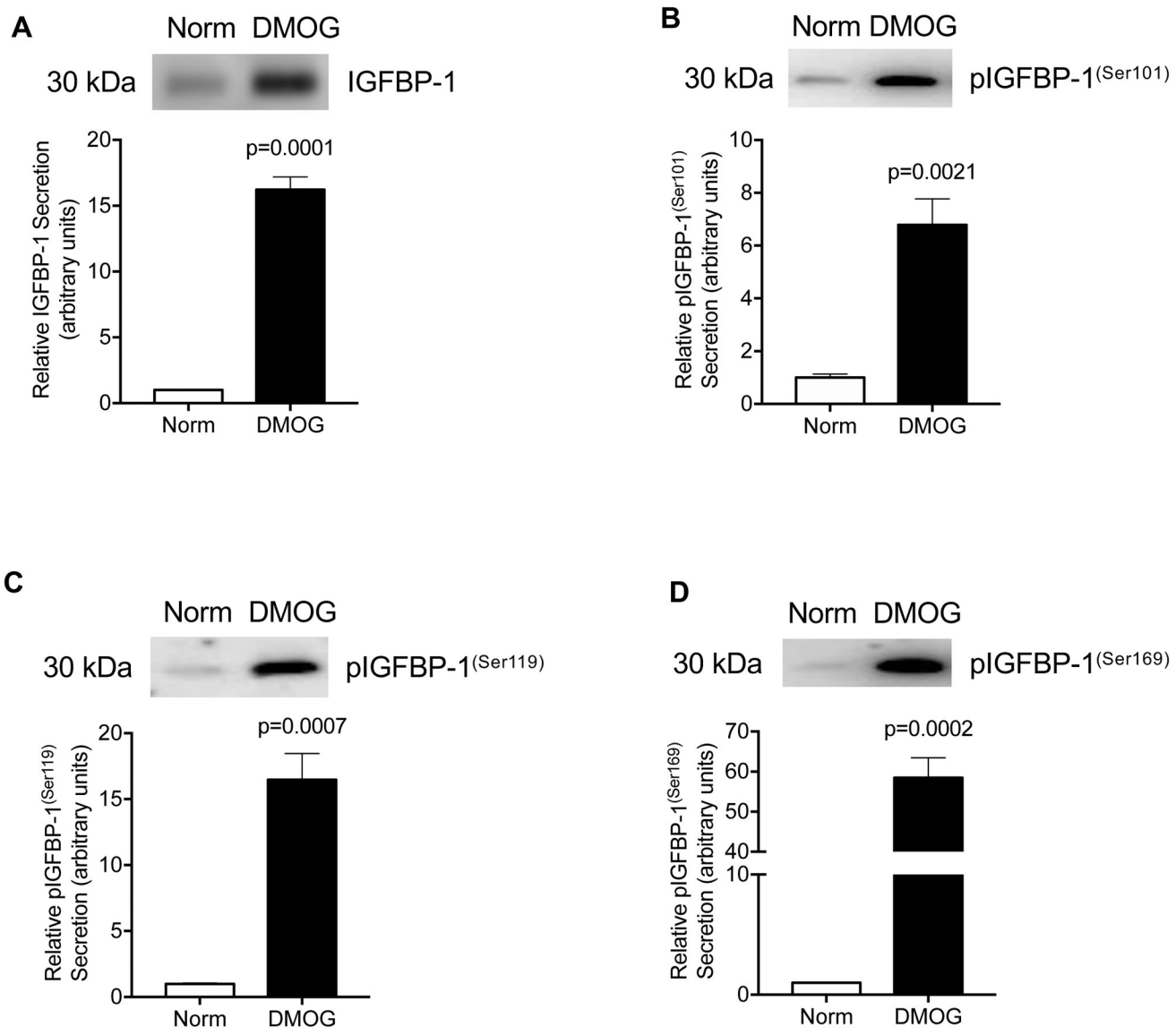

Figure 7. DMOG treatment induces IGFBP-1 secretion and phosphorylation in HepG2 cells in normoxia.

A representative western blot of IGFBP-1 secretion (**A**) in cell media from normoxia (Norm) and normoxia with DMOG (DMOG) treated HepG2 cells. Equal loading (10 μL) was performed.

IGFBP-1 phosphorylation was determined in media from Norm and DMOG-treated HepG2 cells; a representative western blot of IGFBP-1 phosphorylation at Ser101 (**B**), Ser119 (**C**) and Ser169 (**D**) in DMOG-treated HepG2 cell media. Equal loading (30 μL) was performed. Norm (CTR) was assigned a value of 1 (arbitrary units) and DMOG was normalized to Norm to facilitate comparisons between groups. The bar graphs summarize the western blot data as protein secreted in cell media. Values (n=3 each) are displayed as Mean+SEM; unpaired *t*-test, $p<0.05$ considered significant.

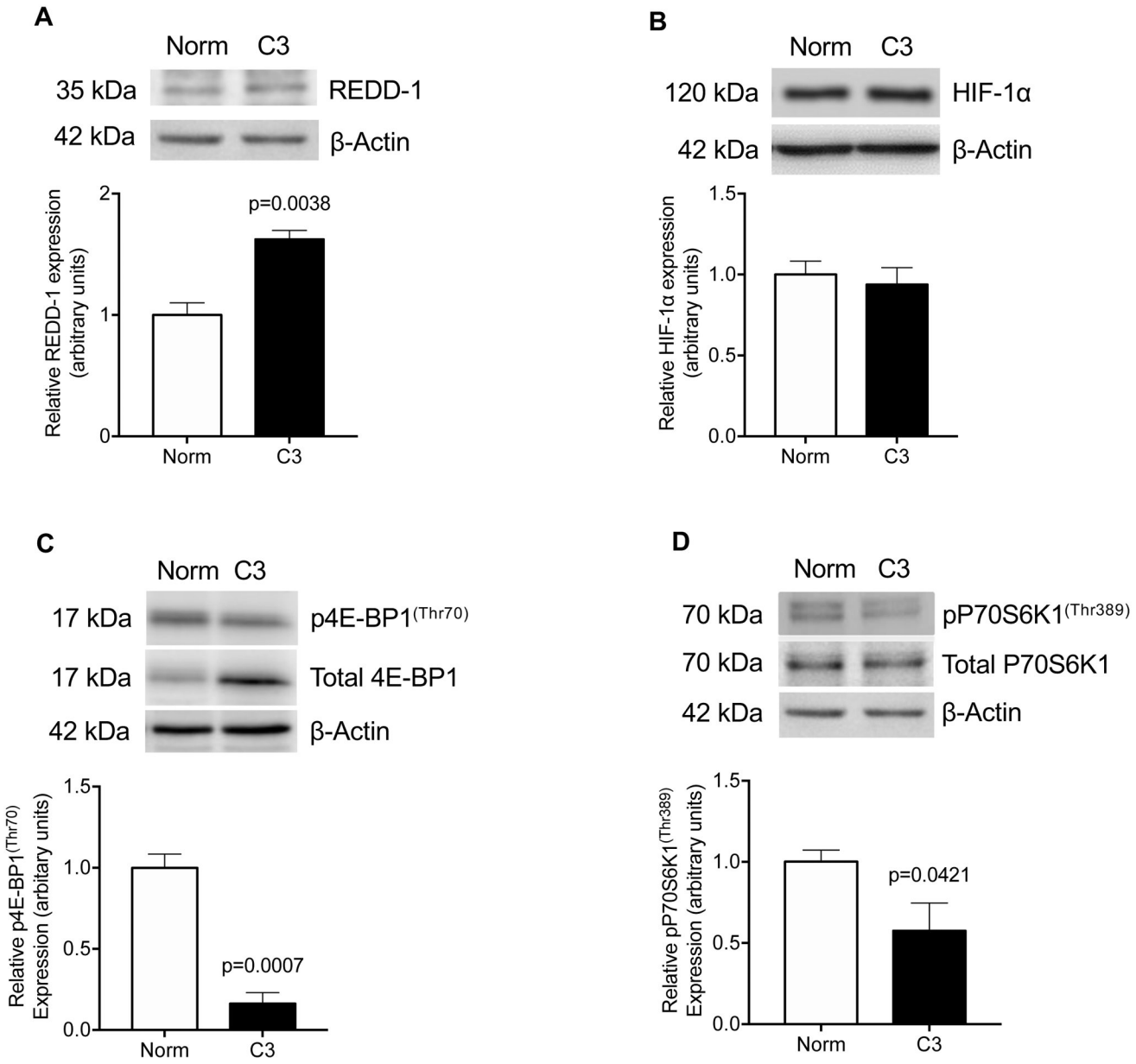

Figure 8. C3 treatment induces expression of REDD-1 and inhibits mTORC1 expression in HepG2 cells in normoxia.

A representative western blot of REDD-1 (**A**) and HIF-1α (**B**) in cell lysate from normoxia (Norm) or normoxia with C3 (C3)-treated HepG2 cells. Equal loading (50 μg) was performed. The bar graphs summarize the western blot data of protein expression with β-actin as the loading control.

A representative western blot of mTORC1 functional readouts 4E-BP1 phosphorylation at Thr70 (**C**) and P70S6K1 phosphorylation at Thr389 (**D**) in cell lysate from Norm or C3-treated HepG2 cells. Equal loading (50 μg) was performed. The bar graphs summarize the western blot data as the ratio of phosphorylated to total protein with β-actin as the loading control.

Control Normoxia (Norm) was assigned a value of 1 (arbitrary units) and C3 was normalized to Norm to facilitate comparisons between groups. Values (n=3 each) are displayed as Mean+SEM; unpaired *t*-test, $p<0.05$ considered significant.

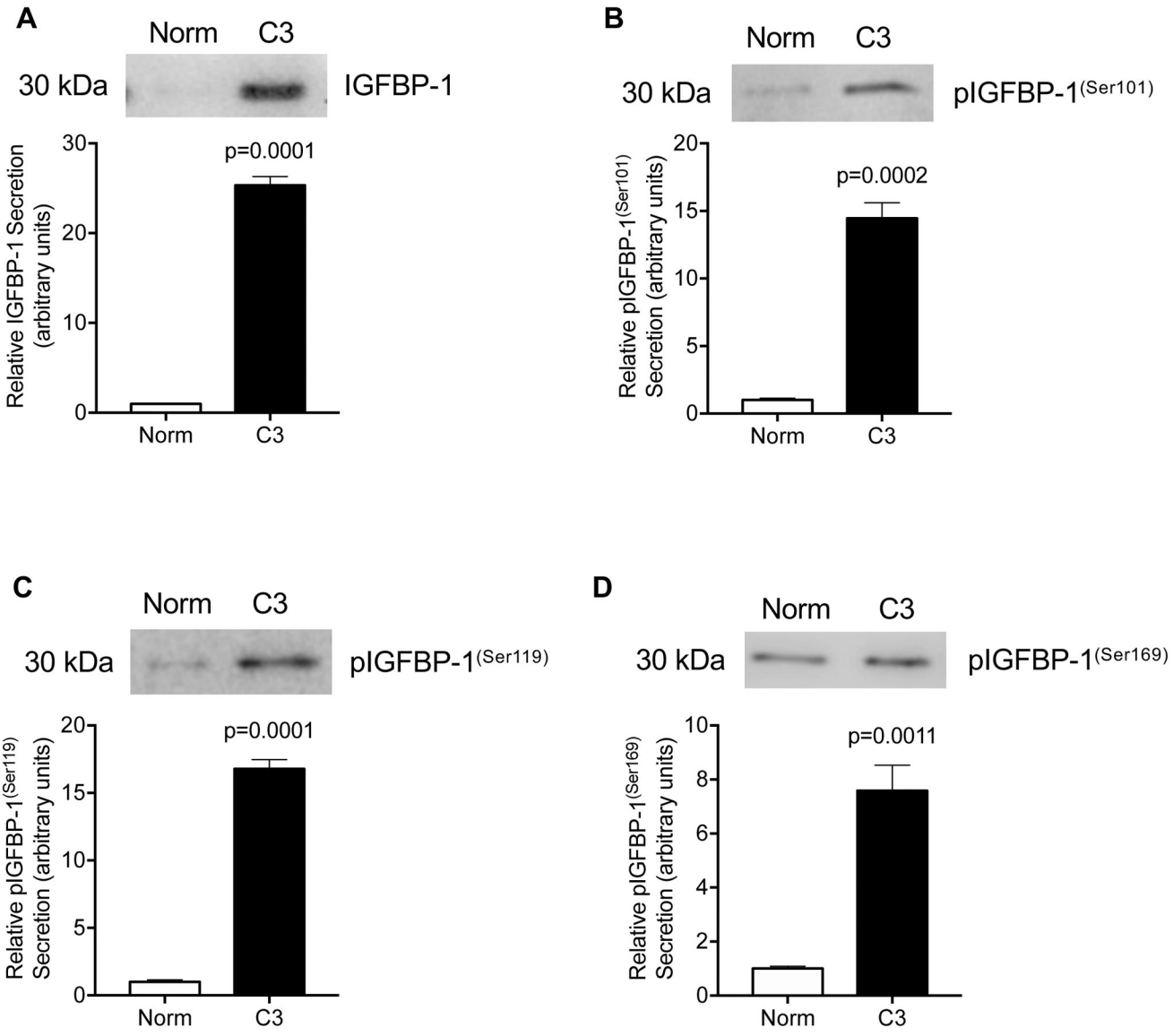

Figure 9. C3 treatment induces IGFBP-1 secretion and phosphorylation in HepG2 cells in normoxia.

A representative western blot of IGFBP-1 secretion (**A**) in cell media from C3 treated HepG2 cells. Equal loading (10 μL) was performed.

IGFBP-1 phosphorylation was determined in media from C3-treated HepG2 cells; a representative western blot of secreted IGFBP-1 phosphorylation at Ser101 (**B**), Ser119 (**C**) and Ser169 (**D**). Equal loading (30 μL) was performed.

Normoxia (Norm) was assigned a value of 1 (arbitrary units) and C3 was normalized to Norm to facilitate comparisons between groups. The bar graphs summarize the western blot data as protein secreted in cell media. Values (n=3 each) are displayed as Mean+SEM; unpaired *t*-test, $p<0.05$ considered significant.

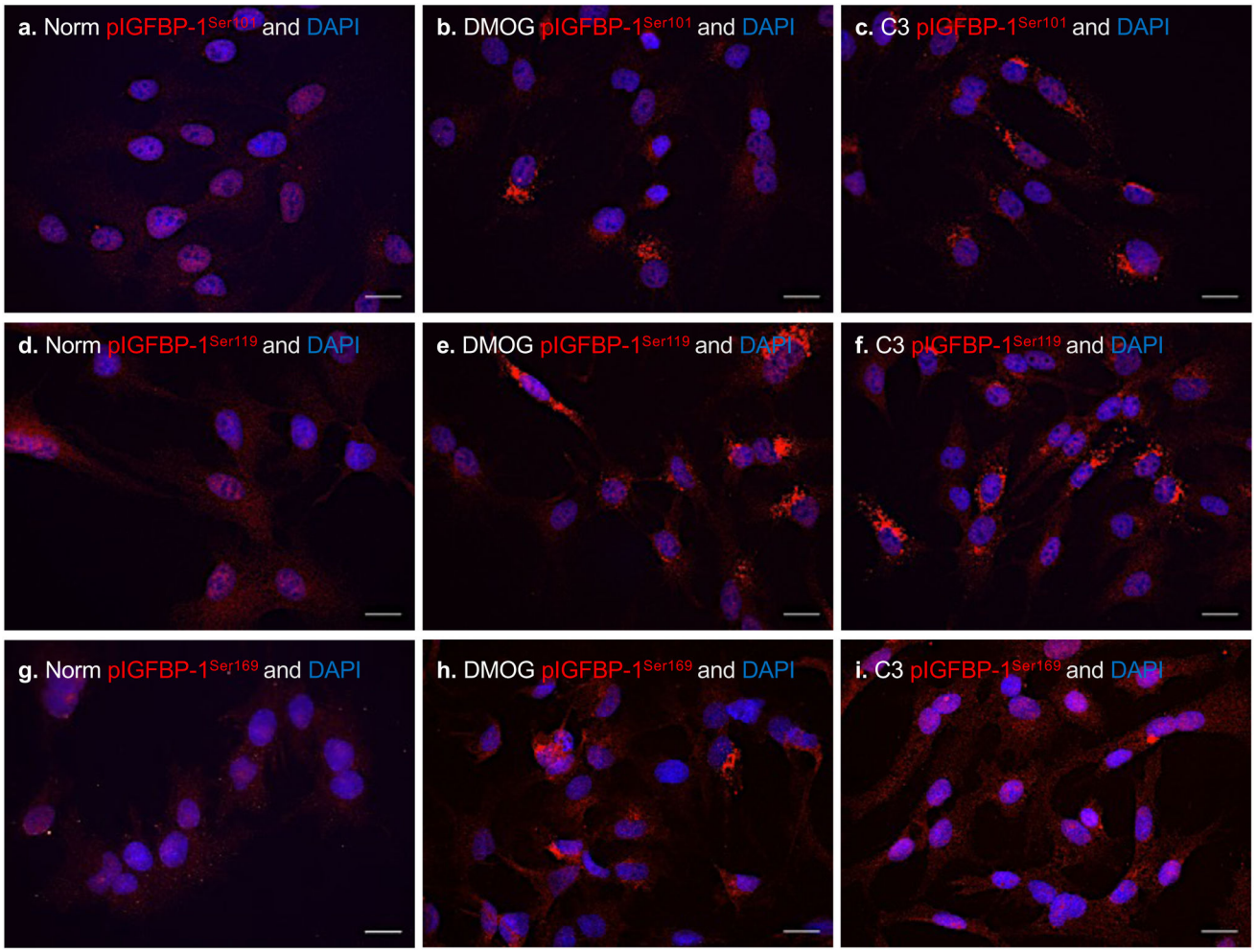

Figure 10. DMOG and C3 treatments increase IGFBP-1 phosphorylation in HepG2 cells in normoxia as determined with immunofluorescence.

Representative immunofluorescence (IF) images for expression of IGFBP-1 phosphorylation at Ser101 (red staining) in HepG2 cells cultured in Normoxia (Norm) (**a**) or treated with DMOG (**b**) or C3 (**c**) in normoxia.

Representative IHC images for expression of IGFBP-1 phosphorylation at Ser119 (red staining) in Norm (**d**), DMOG (**e**) and C3 (**f**) treated HepG2 cells.

Representative IHC images for expression of IGFBP-1 phosphorylation at Ser169 (red staining) in Norm (**g**), DMOG (**h**) and C3 (**i**) treated HepG2 cells in normoxia.

Equal plating of cells was performed. Data is representative of multiple (n=3) images. HepG2 cells were fixed and stained with respective primary and secondary antibodies. DAPI nuclear counterstain is shown in blue. 63x magnification is used (original scale bars, 20 μm).

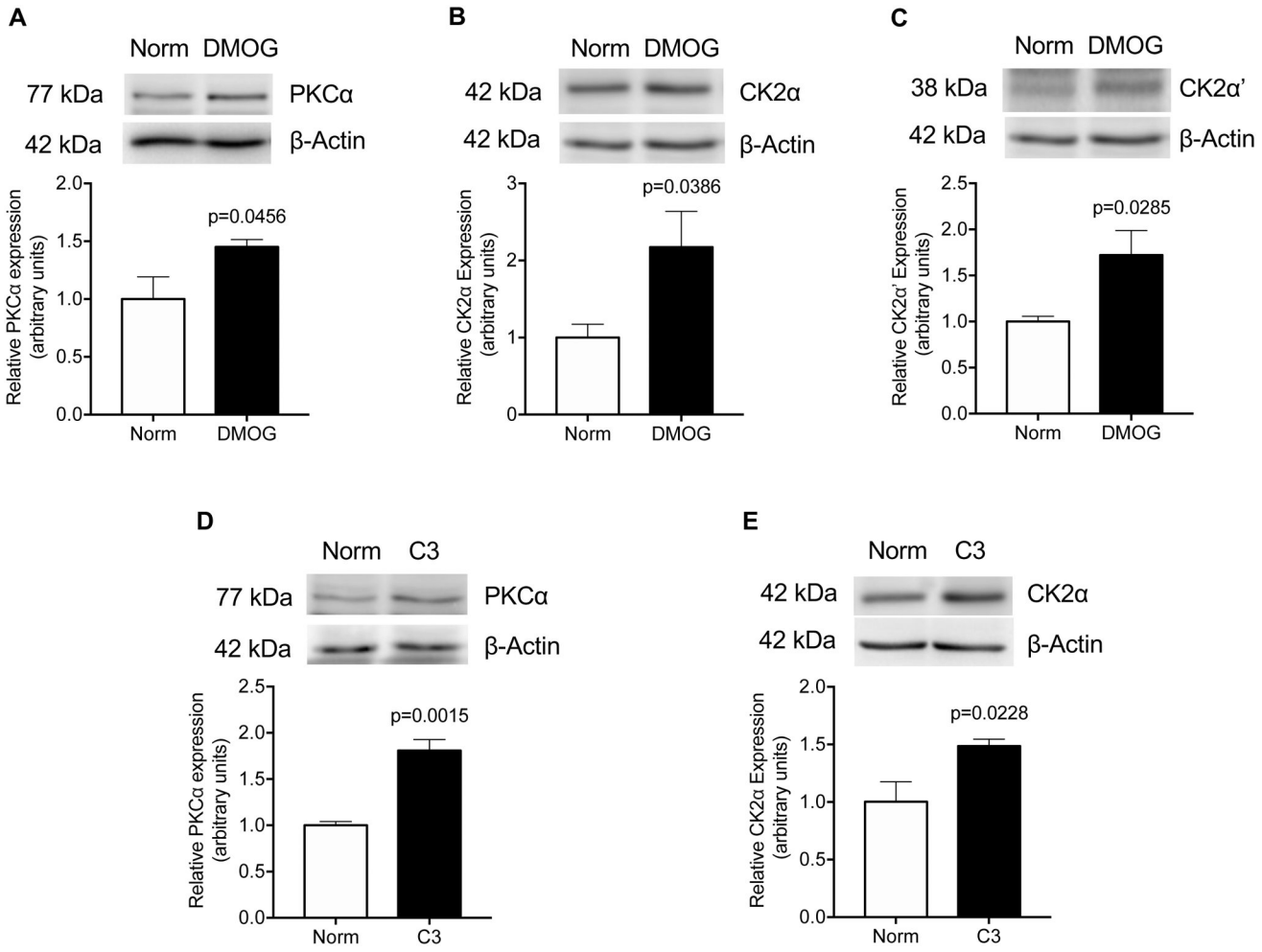

Figure 11. DMOG or C3 treatments increase expression of protein kinases in HepG2 cells in normoxia.

Representative western blots of protein kinase PKCα (**A**), CK2α (**B**), and CK2α' (**C**) expression in cell lysate from DMOG-treated HepG2 cells in normoxia.

Representative western blots of protein kinase PKCα (**D**) and CK2α (**E**) expression in cell lysate from C3-treated HepG2 cells in normoxia.

Equal loading (50 μg) was performed. The bar graphs summarize the western blot data of protein expression with β-actin as the loading control. Normoxia (Norm) was assigned a value of 1 (arbitrary units) and DMOG and C3 were normalized to Norm to facilitate comparisons between groups. The bar graphs summarize the western blot data. Values (n=3 each) are displayed as Mean+SEM; unpaired *t*-test, $p<0.05$ considered significant.

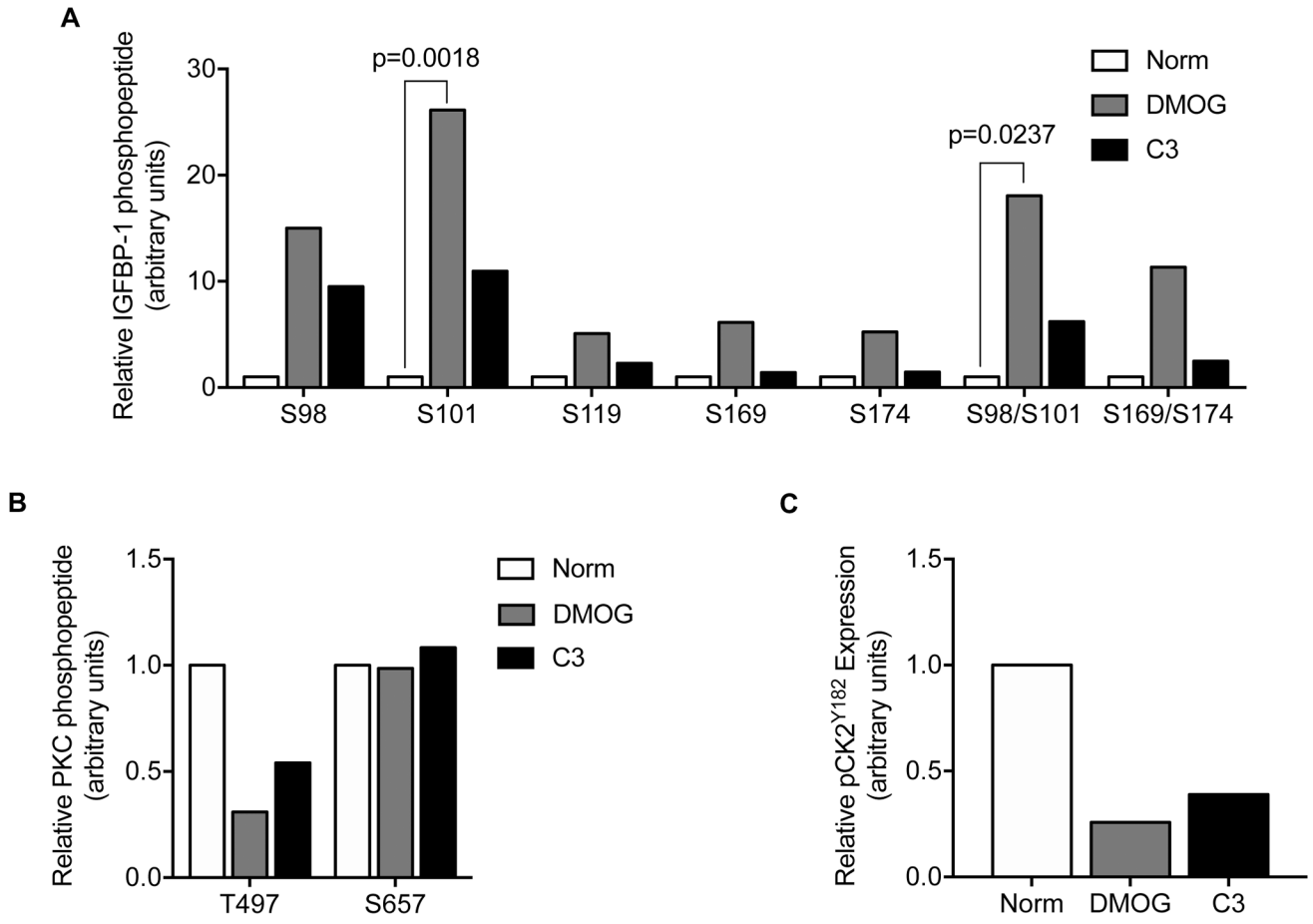

Figure 12. HIF-1α induction increases IGFBP-1 phosphorylation at Ser101 and dually at Ser98+101 sites in HepG2 cells as assessed by PRM-MS.

Representation of PRM-MS data showing relative IGFBP-1 phosphopeptides (**A**), PKC phosphopeptides (**B**), and CK2 phosphopeptides (**C**) in cell lysate from normoxia control (Norm) HepG2 cells or HepG2 cells treated with DMOG or C3. Relative phosphorylation of IGFBP-1 was determined at sites Ser98, Ser101, Ser119, Ser169 singly and dually at Ser98+Ser101 and Ser169+Ser174 (**A**). Relative phosphorylation of PKC was determined at Thr497 and Ser657 (**B**). Relative phosphorylation of CK2 was determined at Tyr182 (**C**). The data is a representation of pooled triplicates from two separate biological treatments. Samples were immunoprecipitated with IGFBP-1 mAb 6303 using cell lysate with 200 μg protein. Bar graphs summarize data of total transition peak intensity relative to untreated normoxia (Norm) samples (set to a value of 1) and normalized to a non-phosphorylated peptide within the IGFBP-1 protein, PKC and CK2. Values are displayed as mean, $p<0.05$ is considered as significant; Two-way ANOVA, corrected with Bonferroni's Multiple Comparisons Test.

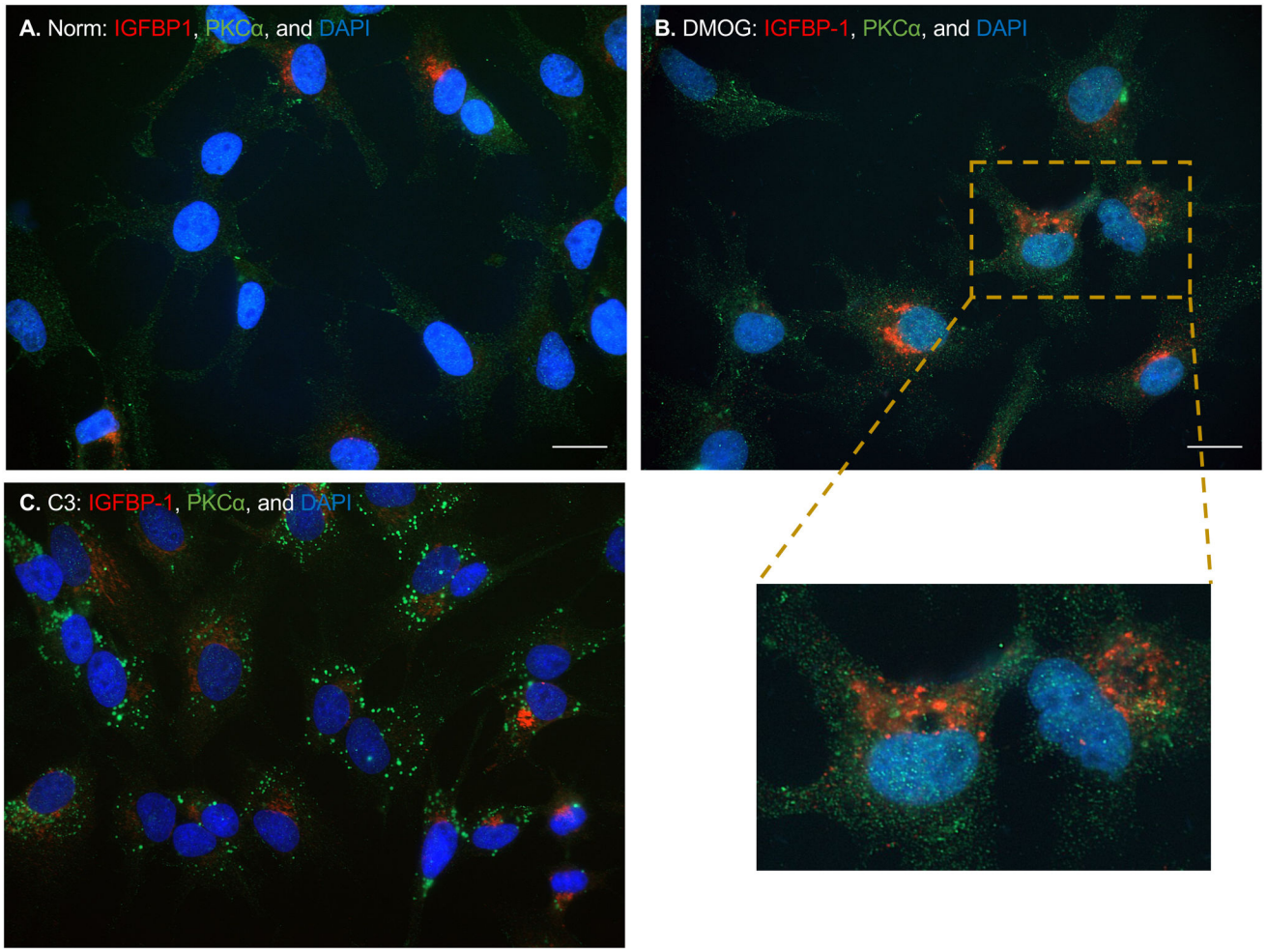

Figure 13. DMOG and C3 treatments increase IGFBP-1 and PKCα expression in HepG2 cells as determined with dual immunofluorescence.

Representative dual immunofluorescence (IF) images for the expression of IGFBP-1 (red staining) and PKCα (green staining) in HepG2 cells cultured under Normoxia (Norm) (**A**) or treated with DMOG (**B**) or C3 (**C**) in normoxia. Image of DMOG-treated HepG2 cells (merged) is also shown zoomed-in (dotted yellow box) below the panel to highlight overlapping red/green staining, representing potential co-localization of IGFBP-1 and PKCα (orange staining).

Equal plating of cells was performed. Data is representative of multiple (n=3) images. HepG2 cells were fixed and stained with respective primary and secondary antibodies. DAPI nuclear counterstain is shown in blue. 63x magnification is used (original scale bars, 20 μm).

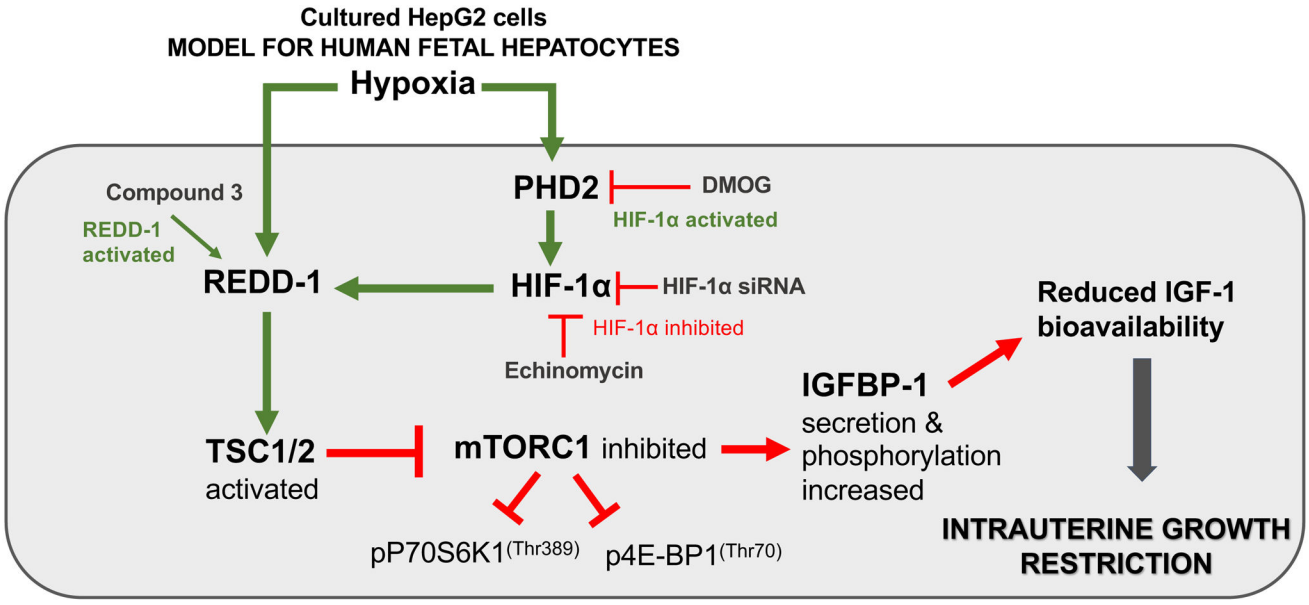

Schematic diagram representing the potential mediators of the HIF-1α pathway that connect to IGFBP1 hyperphosphorylation via mTORC1 in hypoxia. Targets for pharmacological activation and inhibition are presented.

Figure 14. Proposed model of the molecular mechanisms linking fetal hypoxia to reduced fetal growth (intrauterine growth restriction, IUGR).

Functionally important hypoxia-inducible proteins upstream mTOR, linking MNR-induced hypoxia signalling to mTORC1 inhibition and IGFBP-1 hyperphosphorylation.

Key target proteins modulated by hypoxia conditions and/or the addition of pharmacological and siRNA treatments are presented.

Hypoxia-inducible factor 1 (HIF-1), regulated in DNA and development response 1 (REDD-1), erythropoietin (EPO) receptor (EPO-R), vascular endothelial growth factor (VEGF), insulin-like growth factor (IGF) binding protein 1 (IGFBP-1), mechanistic target of rapamycin (mTOR), eukaryotic translation initiation factor 4E-binding protein 1 (4E-BP1), ribosomal protein S6 kinase 1 (P70S6K1).

Table 1.

Fetal and placental weights and cord plasma amino acid concentrations in MNR and Controls baboons at GD120 and GD165.

	GD120			GD165		
	Control n=7	**MNR n=8**	**P-value**	**Control n=7**	**MNR n=10**	**P-value**
Placental weight (g)	139 ± 25	135 ± 20	0.342	207 ± 14	171 ± 12	0.060
Fetal weight (g)	328 ± 58	321 ± 34	0.437	813 ± 37	707 ± 26	0.030
Fetal liver weight (g)	9.72 ± 0.8	10.6 ± 1.2	0.147	24.0 ± 5.2	19.7 ± 1.6	0.043
Serum leucine (μM)	119 ± 24	92.6 ± 18	0.045	108 ± 23	73.6 ± 7.0	0.010
Serum isoleucine (μM)	92.9 ± 22	70.9 ± 8.8	0.018	77.7 ± 14	63.2 ± 8.9	0.160
Serum phenylalanine (μM)	68.1 ± 12	63.5 ± 13	0.450	98.6 ± 16	63.2 ± 11	0.003